天津中德应用技术大学
Tianjin Sino-German University of Applied Sciences

本科生毕业设计

立式加工中心定位精度误差快速检测与补偿方法研究

Research on Rapid Detection and Compensation Method of Positioning Accuracy Error in Vertical Machining Center

姓　　名 张轩荣

学　　院 机械工程学院

专　　业 机械电子工程

指导教师 左维

职　　称 教授

完成时间 **2023 年 5 月**

天津中德应用技术大学

本科生毕业设计（论文）的声明

本人郑重声明：所呈交的毕业设计（论文），是本人在指导教师指导下，进行研究工作所取得的成果。除文中已经注明引用的内容外，本毕业设计（论文）的研究成果不包含任何他人创作的、已公开发表或没有公开发表的作品内容。对本设计（论文）所涉及的研究工作做出贡献的其他个人和集体，均已在文中以明确方式标明。本毕业设计（论文）原创性声明的法律责任由本人承担。

毕业设计（论文）作者签名：

年　月　日

本人声明：该毕业设计（论文）是本人指导学生完成的研究成果，已经审阅过设计（论文）的全部内容，并能够保证题目、关键词、摘要部分中英文内容的一致性和准确性。

毕业设计（论文）指导教师签名：

年　月　日

摘 要

伴随着数控加工技术的不断发展，对机床精度的要求也不断提高，因此，更加需要精度更高、速度更快的测量与补偿方式，本篇论文对激光干涉仪的快速对光实验，螺距误差参数快速补偿宏程序的编写以及两者的应用进行研究。首先，传统的激光干涉仪对光过程占用了其绝大部分的使用时间，其操作过程纷繁芜杂并且对光时间非常不稳定。其次，在 FANUC 系统中，需要进行误差补偿输入的相关参数离散分布在不同的界面，除了输入参数时调整界面花费过多时间外，还非常容易出现少补或错补的现象。综合上述两部分所言，本篇论文研究的内容是一种新的对光方法以及快速螺距误差补偿所适用的宏程序。

本篇论文介绍了雷尼绍（Renishaw）激光干涉仪的各类组件，研究了激光干涉仪的工作原理。对带有 FANUC 0i Mate-MD 数控系统的 YL569 型加工中心进行分析，查阅机床规格参数。推导了检测光路误差模型，研究了新的对光方法，搭建激光干涉仪测量组件，进行了误差测量实验，完成了对螺距误差参数补偿宏程序的编写与应用，进行了对照实验，并完成了对上述理论与方法的验证。

本篇论文针对于激光干涉仪使用的对光过程以及螺距误差的参数设定和螺距误差的数据补偿进行研究与改进。通过本篇论文实验，分别得出新的对光方法时长比传统方法时长在 X 轴上改善了 60.23%，在 Y 轴上改善了 59.69%，在 Z 轴上改善了 59.73%；自动补偿时长比手动补偿时长在 X 轴上改善了 55.85%，在 Y 轴上改善了 53.27%，在 Z 轴上改善了 57.73%。通过本篇论文研究成果的应用可以有效降低对光过程与设定补偿参数过程所占用的时间，并且降低失误率，提高调试效率。因此，本篇论文研究成果对于数控机床定位精度的快速检测与自动输入误差补偿值具有一定的应用价值。

关键词：激光干涉仪；光路准直；误差补偿；宏程序；FANUC

ABSTRACT

With the continuous development of CNC machining technology, the precision of machine tools is also improving, therefore, there are more need for higher precision, faster measurement and compensation methods. This paper carry out research on the laser interferometer fast laser beam focusing experiment and the macro program of fast pitch error parameters compensation and the application of the two studies. Traditional laser interferometers occupy the vast majority of their usage time for the optical process, and their operation process is complex and unstable for the optical time. In the FANUC system, the relevant parameters that need to be input for error compensation are dispersed in different pages, so it takes too much time to adjust the page when input parameters. And it is also very easy to occur the phenomenon of omissive or wrong complement. In summary, this paper researches a new optical method and the macro program needed for fast compensation.

In this paper, various components of Renishaw laser interferometer are introduced and the working principle of laser interferometer is studied. The YL569 machining center with FANUC 0i Mate-MD numerical control system was analyzed to check the product parameters. Derived the error model of detecting optical path, and studied a new optical beam focusing method. Built the laser interferometer measurement module and carried out the error measurement experiment. Complete the writing and application of the macro program for compensating pitch error parameters; A control experiment is carried out to verify the theory and method mentioned above.

In this paper, the optical process and pitch error parameter setting and pitch error data compensation of laser interferometer are studied and improved. Through the application of the experiment in this paper, the time occupied by the optical process and the compensation parameter setting process can be effectively reduced, and the error rate can be reduced and the production efficiency can be improved. The new optical method improves the duration by 60.23% on the X-axis, 59.69% on the Y-axis, and 59.73% on the Z-axis compared to the traditional method, respectively; The automatic compensation duration has improved by 55.85% on the X-axis, 53.27% on the Y-axis, and 57.73% on the Z-axis compared to manual compensation duration. Therefore, this research has certain application value for the fast detection and automatic input error compensation of NC machine tool positioning accuracy.

Key words: Laser interferometer; Laser beam focusing; Error compensation; Macro program; FANUC

目 录

第一章 绪论

1.1 课题研究背景及意义

数控机床作为制造业的加工母机，是我国国民经济的重要基础。自 2006 年以来，国务院、国家发改委以及工信部等多个部门陆续印发了支持并规范数控机床行业的政策，涉及制造业转型升级、数控机床设备规范以及机床国产化等方面内容[1]。其中，数控机床作为工业 4.0 和 “中国制造 2025”步伐推进中的关键要素，同时也面临着激烈的国际市场竞争压力。所以加速推进数控机床的发展是保证我国工业现代化脚步的重要一环。数控机床作为一种大型的零部件加工设备，本身是由多种零部件构建而成的，不可避免的零部件误差将直接影响机床精度；同时，数控机床精度也会直接影响其制造和加工工件的精度以及零部件生产质量。机床精度高低的衡量标准是误差的大小。在不同的生产条件下，其使用者对于机床精度的侧重点也不尽相同。其次，随着机床服役年限逐渐增加，由丝杠老化而引起的反向间隙也会在批量生产中致使加工零部件出现尺寸位移及质量不稳定的问题。为了在不对数控机床硬件进行大幅度改造的条件下提升机床精度，一般要运用激光干涉仪对进行数控机床定位精度的检测与误差补偿。结合目前数控技术发展的实际情况，仍然存在些许不足与欠缺亟待改进[2]。

激光干涉仪是现阶段国内外统一公认的机床位置精度方面的先进检测仪器，雷尼绍 XL80 激光测量系统可以对数控机床以及其他对位置精度有较高要求的设备进行完整且系统的测量与校准，其中也包括对各种几何尺寸和动态机械特性的衡定[3]。然而，在实际的测量检测中，激光干涉仪的对光仍然存在手动操作较难复刻的问题，其过程纷繁芜杂且大多采用经验式调节方法[4]；在 FANUC 系统中，需要进行误差补偿输入的相关数据离散分布在不同页面，容易出现少补或错补的现象。

1.2 国内外研究现状

客观来讲，我国数控机床领域的发展发展周期较短，应用经验积累不够充足，存在由传统模式及固化思维带来的局限性。然而，伴随着改革开放的贯彻落实以及科技强国的现代化脚步持续推进，我国对于机床技术的支持力度也不断上涨。目前阶段，无论是在质量上还是在规模上，我国数控技术的发展已经取得了明显的进步与革新[5]。对于数控机床定位精度以及误差补偿的研究方面，胡安继等[6]利用激光干涉仪当中分光镜与旋转镜的组合，解决了斜导轨机床的倾斜主轴的检测难题。经由光栅尺运动传感器对机床的位置补偿，使机床运动定位精度提升近十倍，使机床加工性能大幅改善。薛邵文[7]通过运用三因素双指标试验来判断数控铣床定位误差与补偿。贾平平[8]通过运用激光干涉仪对水平轴连接杆的形变量进行勘测，根据勘测结果重新设计了其结构，实现了较高的精度补偿以及测量过程的稳定。蒋兴兴[9]认为激光干涉仪是现阶段可以有效测量数控机床定位误差和反向间隙的设备。

自 1960 年 Theodore H. Maiman 研制成功第一台红宝石激光器起，激光干涉测量被广泛地用于长度、角度、微观形貌、转速、光谱等领域。发展至目前，国外针对于数控机床的激光干涉测量技术方法丰富[10]。例如 Jean-Marc 等[11]探讨了运用多边法激光跟踪干涉对 CNC 进行精度补偿的应用问题，其中包含对于不同的测量方法与测量值的热漂移补偿。结果表明：其软件可以准确补偿因温度而带来机床精度方面的大部分影响，但是实验附件的热漂移并未考虑在内，因而其实验结果并未完全修正。为确保该策略的准确性，Jean-Marc 等选择使用五种测量方式对相同机床的误差进行测算，并保证每一种测量方式均为独立制定与执行。总之，这一标准适用于讨论后续研究的程序。Maruyama 等[12] 提出了一种利用激光干涉仪来识别其平面内两个直线轴的二维(2D)误差运动的方案。与传统的激光干涉不同,该方案仅需要安装激光干涉仪器的数控转台。该转台根据指令目标位置调节激光光束的方向，除了直接测量两直线轴的线性定位误差之外，还提出了只需进行一次干涉试验来识别两直线轴的二维误差运动的补偿方法。给出了估计误差运动与直接测量的数据比较。

综上，此前国内外学者、工程师、技术人员以及相关从业者已经在数控机床精度测定与补偿研究领域开辟了较为完整的应用体系。其中，激光干涉测量作为该领域中的重要板块，其测定精确性受到国内外学者的一致认可。

1.3 主要研究内容

本文主要运用激光干涉仪进行快速对光研究并测定 YL569 型加工中心水平轴、垂直轴的定位精度，根据测定数据得出水平轴、垂直轴定位精度的误差，并通过编写宏程序对螺距误差补偿相关参数进行快速改写以达到更便捷地减少该误差所带来的影响。本篇论文各章节的安排如下：

第一章：概述本篇论文对加工中心定位精度快速检测与补偿的研究意义，对比分析国内外研究现状，说明本次课题所运用的技术路线，从而引出本篇论文的研究内容。

第二章：分析数控机床定位误差理论，概括经典的机床定位精度的检测方法，并建立定位误差理论数学模型，回顾并总结激光干涉仪快速对光的规律以及针对于 YL569 型加工中心定位误差快速补偿的方法，编写对螺距误差参数的快速分配与补偿的宏程序。

第三章：对 YL569 型加工中心水平轴与垂直轴的定位误差测量进行实验，对数据结果进行分析与验证。

第四章：得出实验结论，并对未来进行展望。

1.4 技术路线

本篇论文的技术路线，如图 1-1 所示。

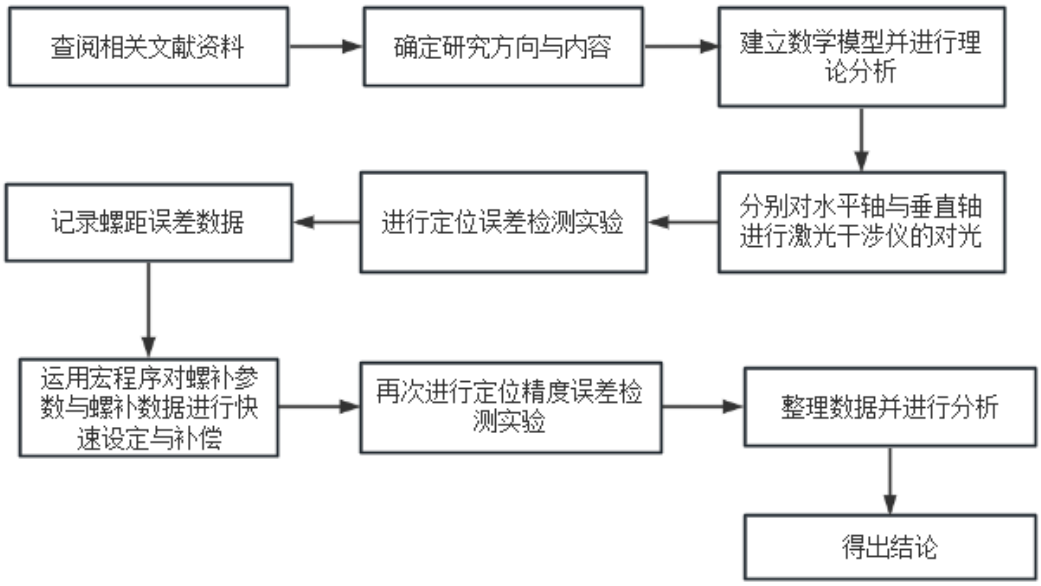
查阅相关文献资料
确定研究方向与内容
建立数学模型并进行理论分析
分别对水平轴与垂直轴进行激光干涉仪的对光
进行定位误差检测实验
记录螺距误差数据
运用宏程序对螺补参数与螺补数据进行快速设定与补偿
再次进行定位精度误差检测实验
整理数据并进行分析
得出结论

图 1-1 技术路线

第二章 光路准直理论及快速补偿研究

2.1 加工中心的基本几何误差分析

为了提高数控机床的加工精度，通常要进行误差分析与补偿。其中，机床误差包括加工误差、机床空间几何误差和热误差等[13]；其中加工中心的基本几何误差包括 21 项几何误差，即 3 项定位误差、6 项线性误差、9 项角度误差以及三轴互相之间的 3 项垂直度误差[14,15]。本课题主要对上述 21 项几何误差中的 3 项定位误差进行研究。

2.2 经典的机床定位精度检测方法

根据国家标准 GB/T 17421.2-2016《机床检验通则 第 2 部分：数控轴线的定位精度和重复定位精度的确定》以及国际标准化组织的规范下，对于数控机床定位精度的检测，应以激光测量为标准。在没有激光干涉仪的情况下，一般也可以使用标准刻度尺，加以光学读数显微镜进行对比测量。但是需要注意的是，测量仪器精度必须比被测的精度高 1~2 个等级[16]。

除了激光干涉仪之外，还有一种精确度高、对测量环境要求不严格并且价格较为低廉的机床定位精度检测工具，名为“步距规”。在机床定位精度检测当中，检测人员常常根据现场情况选择使用“步距规单独测量”或者“结合激光干涉仪进行测量”。其后者的检测结果准确性大幅增高[17]。

2.3 激光干涉仪光路准直分析

2.3.1 激光干涉仪工作原理

当两束频率相同的光相遇，其振幅叠加，则会出现“暗—明—暗”的条纹，这种现象被称为光的干涉。激光头的发射器发射出激光（He-Ne），经由分光镜后被分为两束频率相同的光，先后经两个反射镜反射回到激光头的感应器，并由激光头的检波器检测该两束光的干涉状态，如图 2-1 所示[18]。

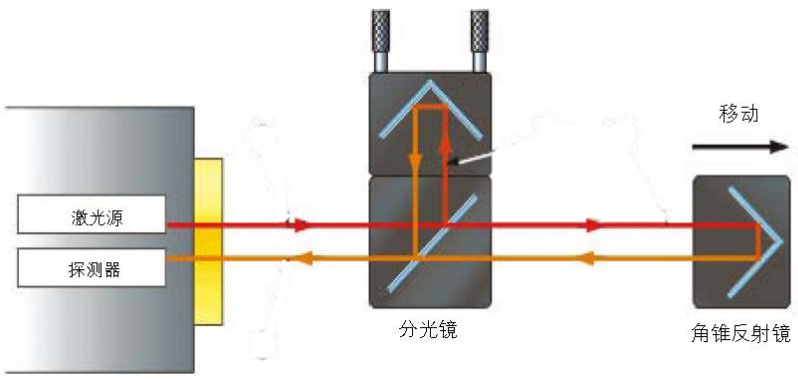

图 2-1 激光干涉仪线性测量原理图

2.3.2 激光干涉仪检测光路误差模型（以 Y 轴为例）

从激光头发射出的激光相对激光头坐标系 O_l-$X_lY_lZ_l$ 沿着 Y 轴到达分光镜坐标系 O_s-$X_sY_sZ_s$，又经分光镜分为两束光，其中一束光到达移动的反射镜坐标系 O_f-$X_fY_fZ_f$，另外一束光经过固定的反光镜后直接返回至激光头的接收器中，如图 2-2 所示。

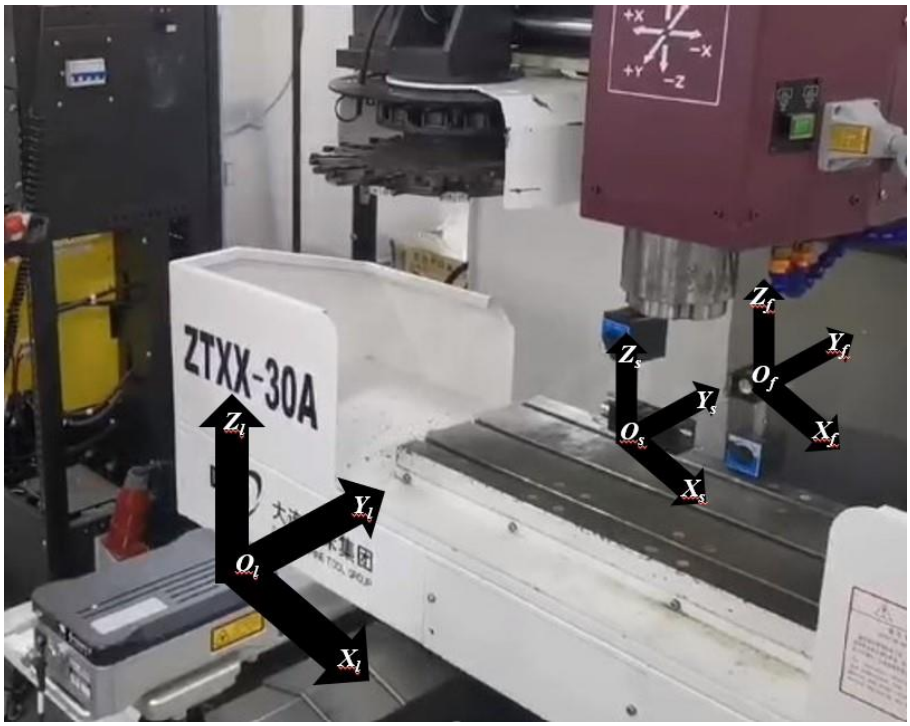

图 2-2 坐标系设定

影响该模型的主要组件误差共有 8 种，如表 2-1 所示。

表 2-1 影响光路的主要组件误差

激光头*(l)*	分光镜*(s)*	移动反射镜*(f)*
$L_x(l)$	$L_x(s)$	$L_x(f)$
$L_z(l)$	—	—
$S_x(l)$	—	—
$S_z(l)$	$S_z(s)$	$S_z(f)$

以激光头发射点为坐标系中心，以激光头处的理想矩阵为单位矩阵：

$$I_l = I_4 \tag{2-1}$$

影响激光头发射的主要误差是来源于沿 X、Z 轴的线性移动以及绕 X、Z 轴的旋转而产生的组件误差。其中，$\Delta T_{L_x}(l)$是激光头沿 X 轴的定位误差$L_x(l)$的误差变换矩阵：

$$\Delta T_{Lx(l)}=\begin{bmatrix}1 & 0 & 0 & L_x(l)\\ 0 & 1 & 0 & 0\\ 0 & 0 & 1 & 0\\ 0 & 0 & 0 & 1\end{bmatrix} \tag{2-2}$$

$\Delta T_{L_z(l)}$是激光头沿 Z 轴的定位误差$L_z(l)$的误差变换矩阵：

$$\Delta T_{Lz(l)}=\begin{bmatrix}1 & 0 & 0 & 0\\ 0 & 1 & 0 & 0\\ 0 & 0 & 1 & L_z(l)\\ 0 & 0 & 0 & 1\end{bmatrix} \tag{2-3}$$

$\Delta T_{Sx(l)}$是激光头绕 X 轴的偏转误差$Sx(l)$的误差变换矩阵：

$$\Delta T_{Sx(l)}=\begin{bmatrix}1 & 0 & 0 & 0\\ 0 & cosS_x(l) & -sinS_x(l) & 0\\ 0 & sinS_x(l) & cosS_x(l) & 0\\ 0 & 0 & 0 & 1\end{bmatrix} \tag{2-4}$$

$\Delta T_{Sz(l)}$是激光头绕 Z 轴的偏转误差$S_z(l)$的误差变换矩阵：

$$\Delta T_{S_z(l)}=\begin{bmatrix}cosS_z(l) & -sinS_z(l) & 0 & 0\\ sinS_z(l) & cosS_z(l) & 0 & 0\\ 0 & 0 & 1 & 0\\ 0 & 0 & 0 & 1\end{bmatrix} \tag{2-5}$$

该模型在激光头发射点处的综合误差矩阵为：

$$E_l = \Delta T_{L_x(l)}\Delta T_{L_z(l)}\Delta T_{S_x(l)}\Delta T_{S_z(l)}I_l \tag{2-6}$$

即：

$$E_l=\begin{bmatrix}cosS_z(l) & -sinS_z(l) & 0 & L_x(l)\\ cosS_x(l)sinS_z(l) & cosS_x(l)cosS_z(l) & -sinS_x(l) & 0\\ sinS_x(l)sinS_z(l) & cosS_z(l)sinS_x(l) & cosS_x(l) & L_z(l)\\ 0 & 0 & 0 & 1\end{bmatrix}$$

当激光从激光头处发射至分光镜处时，其理想矩阵为：

$$I_S=\begin{bmatrix}1 & 0 & 0 & 0\\ 0 & 1 & 0 & y_1\\ 0 & 0 & 1 & 0\\ 0 & 0 & 0 & 1\end{bmatrix} \tag{2-7}$$

影响分光镜处的主要误差是沿分光镜 X 轴的线性移动以及绕其 Z 轴的旋转而产生的组件误差。其中，$\Delta T_{L_x(\mathrm{s})}$是激光沿分光镜 X 轴线性移动而产生的定位误差$L_x(\mathrm{s})$的误差变换矩阵：

$$\Delta T_{L_x(s)}=\begin{bmatrix}1 & 0 & 0 & L_x(s)\\ 0 & 1 & 0 & 0\\ 0 & 0 & 1 & 0\\ 0 & 0 & 0 & 1\end{bmatrix} \tag{2-8}$$

$\Delta T_{S_z(s)}$是激光绕分光镜 Z 轴的旋转而产生的定位误差$S_z(s)$的误差变换矩阵：

$$\Delta T_{S_z(s)}=\begin{bmatrix}cosS_z(s) & -sinS_z(s) & 0 & 0\\ sinS_z(s) & cosS_z(s) & 0 & 0\\ 0 & 0 & 1 & 0\\ 0 & 0 & 0 & 1\end{bmatrix} \tag{2-9}$$

该模型在分光镜处的综合误差矩阵为：

$$E_s = \Delta T_{L_x(s)}\Delta T_{S_z(s)}I_s \tag{2-10}$$

即：

$$E_s=\begin{bmatrix} cosS_z(s) & -sinS_z(s) & 0 & L_x(s)-y_1 sinS_z(s) \\ sinS_z(s) & cosS_z(s) & 0 & y_1 cosS_z(s) \\ 0 & 0 & 1 & 0 \\ 0 & 0 & 0 & 1 \end{bmatrix}$$

当激光从激光头处发经过分光镜到达移动反光镜处时，其理想矩阵为：

$$I_f=\begin{bmatrix} 1 & 0 & 0 & 0 \\ 0 & 1 & 0 & y_2 \\ 0 & 0 & 1 & 0 \\ 0 & 0 & 0 & 1 \end{bmatrix} \tag{2-11}$$

影响移动反光镜处的主要误差是沿移动反光镜 X 轴的线性移动以及绕其 Z 轴的旋转而产生的组件误差。其中，$\Delta T_{L_x(f)}$是激光沿移动反光镜 X 轴线性移动而产生的定位误差 $L_x(f)$的误差变换矩阵：

$$\Delta T_{L_x(f)}=\begin{bmatrix} 1 & 0 & 0 & L_x(f) \\ 0 & 1 & 0 & 0 \\ 0 & 0 & 1 & 0 \\ 0 & 0 & 0 & 1 \end{bmatrix} \tag{2-12}$$

$\Delta T_{S_z(f)}$是激光绕移动反光镜 Z 轴的旋转而产生的定位误差$S_z(s)$的误差变换矩阵：

$$I_f=\begin{bmatrix} cosS_z(f) & -sinS_z(f) & 0 & 0 \\ sinS_z(f) & cosS_z(f) & 0 & 0 \\ 0 & 0 & 1 & 0 \\ 0 & 0 & 0 & 1 \end{bmatrix} \tag{2-13}$$

该模型在移动反光镜处的综合误差矩阵为：

$$E_f = \Delta T_{L_x(f)} \Delta T_{S_z(f)} I_f \tag{2-14}$$

即：

$$E_f=\begin{bmatrix} cosS_z(f) & -sinS_z(f) & 0 & L_x(f)-y_2 sinS_z(f) \\ sinS_z(f) & cosS_z(f) & 0 & y_2 cosS_z(f) \\ 0 & 0 & 1 & 0 \\ 0 & 0 & 0 & 1 \end{bmatrix}$$

激光到达分光镜处的坐标为：

$$P_s=E_l E_s T \tag{2-15}$$

其中 T=$(0001)^T$，由于该坐标点与前 3 列位置无关，仅与最后一列有关，所以取其最后一列，乘以 T。

即：

$$P_s=\begin{bmatrix} L_x(l)+L_x(s)cosS_z(l)-y_1[sinS_z(s)cosS_z(l)+cosS_z(s)sinS_z(l)] \\ L_x(s)cosS_x(l)sinS_z(l)-y_1 cosS_x(l)[sinS_z(s)sinS_z(l)-cosS_z(s)cosS_z(l)] \\ L_z(l)+L_x(s)sinS_x(l)sinS_z(l)-y_1 sinS_x(l)[sinS_z(l)sinS_z(s)-cosS_z(s)cosS_z(l)] \\ 1 \end{bmatrix}$$

分光镜的齐次坐标为：

$$P_1=\begin{bmatrix} x_s \\ y_s \\ z_s \\ 1 \end{bmatrix} \tag{2-16}$$

所以分光镜的误差应为：

$$\Delta P_s = P_s - P_1 \tag{2-17}$$

激光到达移动反光镜处的坐标为：

$$P_f=E_lE_fT \tag{2-18}$$

即：

$$P_f=\begin{bmatrix} L_x(l)+L_x(f)cosS_z(l)-y_2[sinS_z(f)cosS_z(l)+cosS_z(f)sinS_z(l)] \\ L_x(f)cosS_x(l)sinS_z(l)-y_2cosS_x(l)[sinS_z(f)sinS_z(l)-cosS_z(f)cosS_z(l)] \\ L_z(l)+L_x(f)sinS_x(l)sinS_z(l)-y_2sinS_x(l)[sinS_z(l)sinS_z(f)-cosS_z(f)cosS_z(l)] \\ 1 \end{bmatrix}$$

移动反光镜的齐次坐标为：

$$P_2=\begin{bmatrix} x_f \\ y_f \\ z_f \\ 1 \end{bmatrix} \tag{2-19}$$

所以移动反光镜的误差应为：

$$\Delta P_f = P_f - P_2 \tag{2-20}$$

由于P_s与P_f两点在 X 与 Z 轴的方向上坐标相同，而在移动轴 Y 轴的方向上有一个 k 倍的线性移动量关系，则联立(2-15)与(2-18)，得到P_s与P_f的等式为:

$$\begin{cases} P_s(1,1)=P_f(1,1) \\ P_s(2,1)=kP_f(2,1) \\ P_s(3,1)=P_f(3,1) \end{cases} \tag{2-21}$$

2.4 对光方法研究

一般情况下，除了激光干涉仪器设备的搭建、与 PC 端口的连接以及环境补偿单元的安装之外，传统的激光干涉仪对光过程占用了其绝大部分的使用时间，其操作过程纷繁芜杂并且对光时间非常不稳定。所以，相较于传统的对光方法来说，一种快速且稳定的对光方法可以大幅减少对光所占用的时间，并且使其更具有稳定性。下文将以 Y 轴的线性测量为例，逐一介绍传统的激光干涉仪的对光方法以及一种新的激光干涉仪的对光方法。

2.4.1 传统的激光干涉仪对光方法

传统的激光干涉仪对光过程在完成设备的搭建、与 PC 端口的连接以及环境补偿单元的安装之后，就要进行光学系统的调整及测量，也就是上文中所提到的对光[19,20]。其主要对光过程如下：

1.将激光头预热后使激光头光闸调整至完整光束/光靶状态，如图 2-3 所示。

图 2-3 激光头的完整光束/光靶状态

2.在工作台远端安装带有光靶的反射镜，调整 X 轴以及承载激光头的三脚架中心柱的高度，使得激光照射在光靶上，如图 2-4 所示。

图 2-4 激光照射在光靶上

3.前后移动工作台的 Y 轴，通过旋转激光头的云台以及平移 X 轴，使得激光照射在反光镜光靶的位置不变。

4.取下反光镜上的光靶，使得反射出来的光束照射至激光头光闸的光靶位置；前后移动 Y 轴，通过调整激光头的位置与角度，使反射激光始终照射在激光头光闸的光靶上。

5.将分光镜通过磁力座固定在主轴上，并且保证其不接触主轴的旋转部分，将光靶白点向上安装在分光镜的镜面上；调整分光镜的位置与角度，使得入射激光束照射在光靶上。

6.将光靶取下安装至分光镜后面，调整分光镜的反射光线，使其照射至激光头的光靶位置。

7.取下光靶并调节分光镜，使得分光镜的反射光线与反光镜的反射光线通过分光镜后在激光头的光靶上重合。

8.反复移动 Y 轴，使得近端与远端的激光光线都可以照射至激光头的光靶位置。

9.将激光头调整至“工作”状态，观察其接收信号强度指示灯是否全亮；若强度不足，则重新调节，如图 2-5 所示。

图 2-5 激光头“工作”状态

2.4.2 激光干涉仪对光方法细节优化

2.4.1 中叙述的传统对光方法虽然可以完成激光干涉仪的光路准直，但是其操作过程太过模糊，操作结果也不稳定。所以，本文提出对激光干涉仪的激光头与镜组搭建以及对光过程 4、5 中的“调节激光光线”的操作细化，用以提高其结果稳定度。

1.搭建反光镜与分光镜时，应注意，如图 2-6 所示。

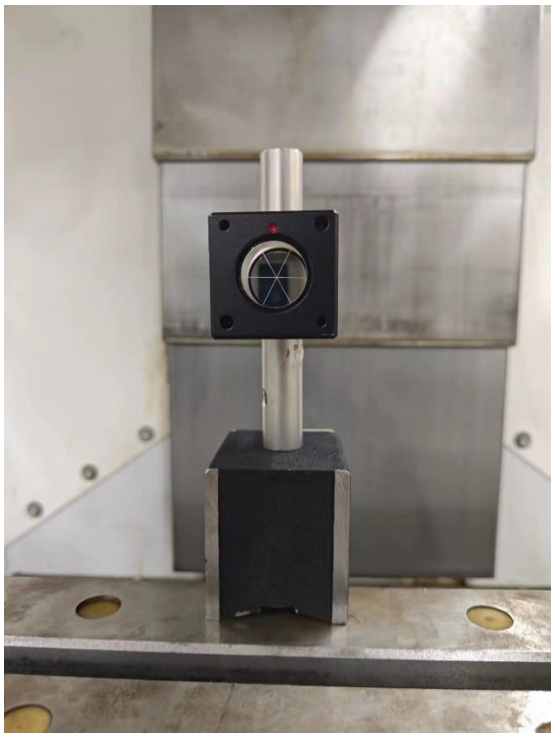

图 2-6 镜框上的红点方向朝上

2.搭建移动反光镜时，可以使用千分表校准移动反光镜与 X 轴的平行度。

3.在搭建激光干涉仪的激光头时，上下调整三脚架后可以用肉眼瞄准激光头中心线与移动反光镜的光靶位置在 Y 轴上是否对齐，如图 2-7 所示。

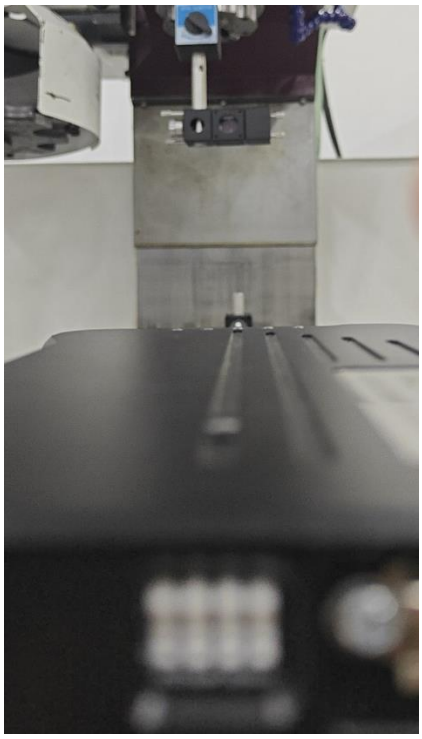

图 2-7 肉眼瞄准激光头中心线与光靶对齐

4.调整 Y 轴，尽量缩短移动反光镜在最前端时与分光镜之间的距离以及分光镜与激光头之间的距离，以减少死程误差，但要注意提前预判机床行程，避免发生碰撞，如图 2-8 所示。

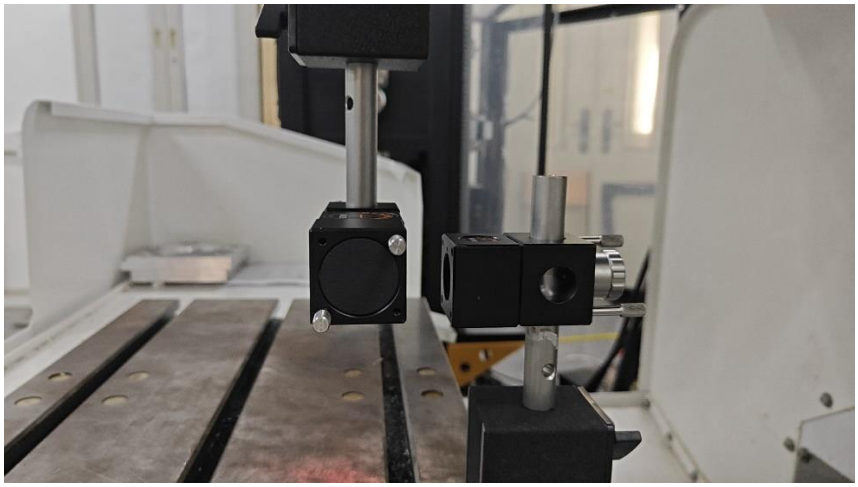

图 2-8 减少死程误差但注意应避免碰撞

5.在移动 Y 轴的过程中，会出现两种情况，分别是“近光点”与“远光点”。其中，前者是随着 Y 轴的移动，移动反光镜距离激光头最近时的状态；而后者则是随着 Y 轴的移动，移动反光镜距离激光头最远时的状态。

(1)当调节过程处于“近光点”状态并且光点不与光靶位置重合时，则进行先水平平移激光头使得光点移动至对称位置，后偏摆激光头回中心，如图 2-9 所示。

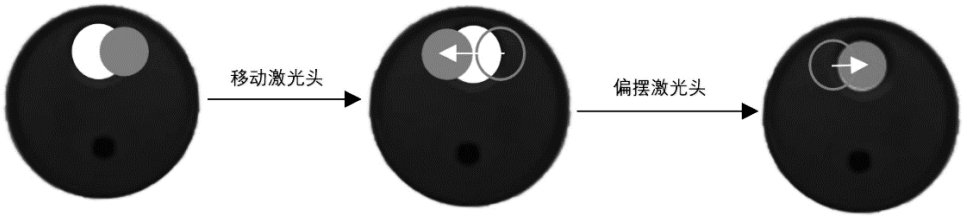

图 2-9 “近光点”调节

(2)当调节过程处于“远光点”状态并且光点不与光靶位置重合时，则先偏摆激光头使光点移动至对称位置，后平移机床 X 轴使光点回中心，如图 2-10 所示。

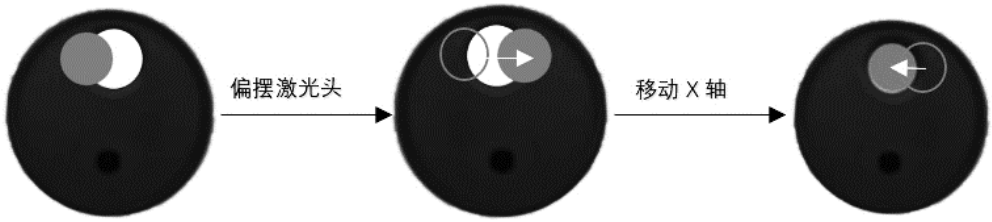

图 2-10 “远光点”调节

6.调节 Y 轴时，若光点移除光靶边缘一半，则停止移动机床，对光回中心。

7.首先完成反光镜的搭建与对光，再进行分光镜的搭建与对光。

8.在进行分光镜的对光时，若在移动 Y 轴的过程中，两束激光光束慢慢分离，不再重合，则应观察以下情况：

(1)当随着 Y 轴的移动，两光点呈现 X 轴方向上的分离，则应微调分光镜的偏摆。

(2)当随着 Y 轴的移动，两光点呈现 Z 轴方向上的分离，则应微调激光头的俯仰，后调整分光镜的垂直位置。

2.5 定位精度参数快速补偿研究

在完成激光干涉仪的搭建、对光与测量之后，会得到一组机床定位精度误差的数据，而后要对机床数据进行补偿[21]。

在 FANUC 系统中，需要进行螺距误差与反向间隙补偿输入的相关参数（即参数 3620、3621、3622、3623、3624、1851）离散分布在不同的界面，使得输入参数时调整界面花费过多时间，还非常容易出现少补或错补的现象，如图 2-11 所示。

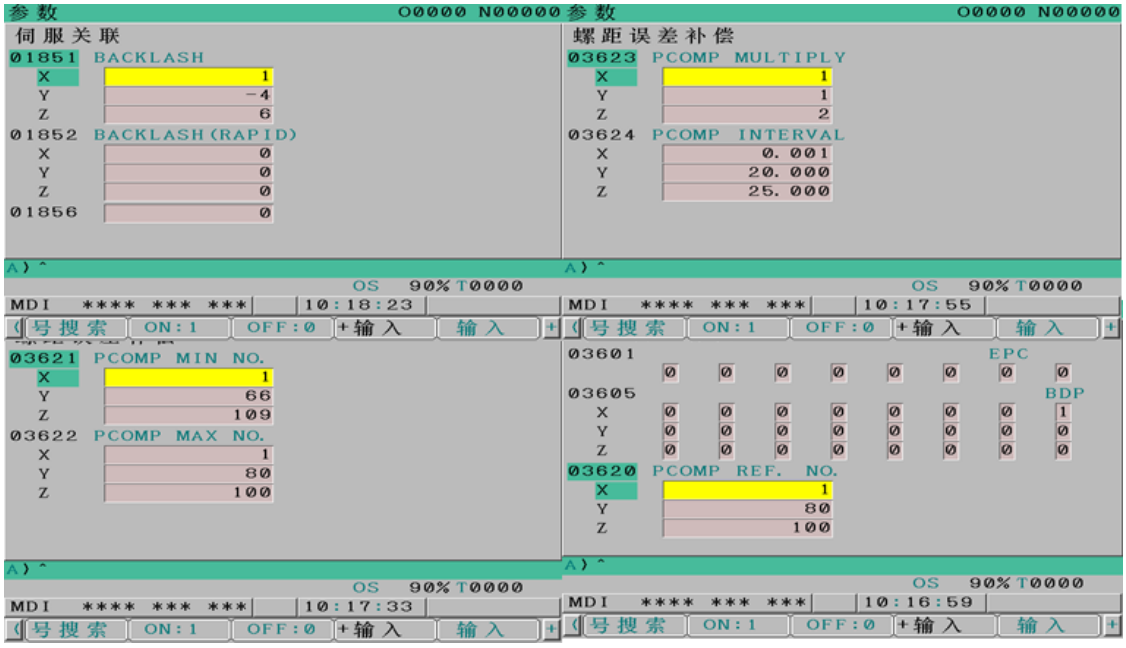

图 2-11 FANUC 系统中需要进行误差补偿输入的相关参数

而在 SIEMENS 系统中，虽然需要进行螺距误差补偿输入的相关参数出现在同一页，但是操作者仍需要切换界面以完成对反向间隙的补偿，并不能够一次完成所有的补偿内容，如图 2-12、2-13 所示。

图 2-12 SIEMENS 系统中螺距误差补偿参数与数据的输入界面

图 2-13 SIEMENS 系统中反向间隙补偿值的输入界面

本课题利用宏程序，在设定时指定其参数并完成数据输入，即可大大缩小所需要的时间并且降低了出错的可能性。完成螺距误差补偿参数的设定，同时应将螺距误差补偿数据输入至相应螺补号位置，即可完成对机床螺距误差的补偿。

为此，本文编写出一套宏程序模板，在完成机床线性测量之后，于 PC 端相应位置输入螺距补偿相关参数以及螺距补偿数据的数值并通过 PCMCIA 卡导入机床，在机床端运行该程序即可完成参数的自动设定和螺距误差补偿数据的自动输入，完整程序设计及中英文注释见附录二。

此处介绍该宏程序的架构范式：

%

O8010；

G10L52；（设定参数输入方式）

N11502R00001100；（执行宏程序调用和可编程参数输入高速执行）

#1=_（X 轴为 1，Y 轴为 2，Z 轴为 3）

N3620P#1R_；（某轴参考点的螺距补偿点号）

N3621P#1R_；（某轴负方向最远端的螺距补偿点号）

N3622P#1R_；（某轴正方向最远端的螺距补偿点号）

N3623P#1R_；（某轴螺距补偿倍率）

N3624P#1R_；（某轴螺距补偿点的间隔）

N1851P#1R_；（某轴反向间隙补偿量）

G11；（取消参数输入方式）

G10L50；（设定螺距输入方式）

N_R_；（起始相应螺补号的螺距补偿量）

N_R_；（起始相应螺补号+1 的螺距补偿量）

N_R_；（起始相应螺补号+2 的螺距补偿量）

……

N_R_；（结束相应螺补号的螺距补偿量）

G11；（取消螺距输入方式）

M30；

%

说明：在 G10L52 中，在 R 后的下划线处填入该参数的设定值；在 G10L50 中，在 N 后的下划线处填入相应螺补号（由程序中 3620、3621、3622 等参数决定），在 R 后的下划线处填入相应的螺补数据。

例如，对 X 轴测量的补偿宏程序及中英文注释：

%

O8010；

G10L52；（设定参数输入方式）

#1=1（选择轴为 X 轴）(X axis)

N11502R00001100；（执行宏程序调用和可编程参数输入高速执行）

N3620P#1R30；（X 轴参考点的螺距补偿点号为 30）(NO. of PITCH for X)

N3621P#1R21；（X 轴负方向最远端的螺距补偿点号为 30）(NO. of PITCH for -X)

N3622P#1R30；（X 轴正方向最远端的螺距补偿点号为 21）(NO. of PITCH for +X)

N3623P#1R1；（X 轴螺距补偿倍率为 1）(Magnification of PITCH for X)

N3624P#1R35；（X 轴螺距补偿点的间隔为 35）(Interval of PITCH for X axis)
N1851P#1R-1；（X 轴反向间隙补偿量为-1）(X axis backlash)
G11；（取消参数输入方式）
G10L50；（设定螺距输入方式）
N21R-6；（21 号螺距补偿量）(No. 21 data)
N22R-6；（22 号螺距补偿量）(No. 22 data)
N23R-6；（23 号螺距补偿量）(No. 23 data)
N24R-7；（24 号螺距补偿量）(No. 24 data)
N25R-7；（25 号螺距补偿量）(No. 25 data)
N26R-7；（26 号螺距补偿量）(No. 26 data)
N27R-7；（27 号螺距补偿量）(No. 27 data)
N28R-6；（28 号螺距补偿量）(No. 28 data)
N29R-7；（29 号螺距补偿量）(No. 29 data)
N30R-7；（30 号螺距补偿量）(No. 30 data)
G11；（取消螺距输入方式）
M30；
%

第三章 定位精度误差检测与补偿实验

3.1 实验设备简介

3.1.1 YL569 型加工中心介绍

YL569 型加工中心组成：FANUC 0i Mate-MD 数控系统和 ZTXX-30A 机械本体，工作台尺寸为 700×320mm，X 轴行程为 450mm，Y 轴行程为 350mm，Z 轴行程为 380mm，如图 3-1 所示。

图 3-1 YL569 型加工中心

YL569 型加工中心所配备的电气控制单元（数控装置、电气控制柜、伺服驱动系统等）主要技术参数，如表 3-1 所示。

表 3-1 YL569 加工中心电气控制单元参数表

序号	硬件名称	型号（简要参数）
1	数控系统	FANUC Series 0i Mate-MD
2	I/O 板	KCC-REM-FRR-C62
3	伺服放大器	βisvsp 20/20/40-11
4	伺服放大器风扇	无
5	主轴电机	βiI 8/10000
6	X 轴电机	βiSc 8/3000
7	Y 轴电机	βiSc 8/3000
8	Z 轴电机	βiSc 12/3000
9	驱动单元	FANUC βiSVSP20-20/7.5
10	手轮单元	手摇脉冲发生器
11	电源	三相五线 AC 380V±10% 50Hz
12	漏电保护	漏电动作电流≤30mA
13	数控控制台尺寸	长（mm）×宽（mm）×高（mm）＝800×600×1800

3.1.2 雷尼绍（Renishaw）激光干涉仪介绍

雷尼绍（Renishaw）激光干涉仪检测设备包括一个分射光的分光镜，两个用来反射光的线性反射镜，一个 XL-80 激光器，一个用来支撑激光干涉仪的三脚架，一个雷尼绍 XC-80 环境补偿单元、一个检测材料温度的温度传感器和一个检测空气温度的温度传感器，如图 3-2 所示。

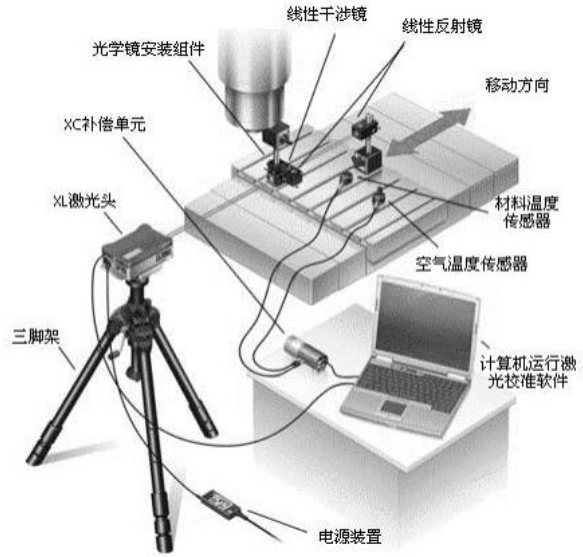

图 3-2 激光干涉仪

3.2 对 X 轴定位精度误差测量实验

3.2.1 对 X 轴定位精度误差测量中搭建设备与对光的过程

1.对 X 轴进行实验设备的搭建

（1）三脚架的安装与调平

安装三脚架时，将其放置在坚硬的地面上，注意不要放在可移动机床脚踏板或木质零件上，伸出伸缩式三脚架到所需要的长度后锁定。其高度设定应该使得激光光束正投射至光学镜组元件上。将水平泡放置在三脚架云台上，调整三脚架水平，将激光头固定至云台上并锁定云台。粗调激光头准直，使得其大致指向测量光学元件。

（2）镜组的安装与固定

线性测量镜组由一个分光镜、一个移动反光镜、一个固定反光镜以及两个光靶组成，根据不同测量轴应选用适当的夹具将其固定至相应位置，如图 3-3 所示。

图 3-3 对 X 轴螺距误差测量中设备搭建图

（3）补偿单元的搭建与激光头的预热

将材料温度、环境补偿单元吸附在机床固定处，并将补偿单元与激光头连接至 PC 端；打开激光头，将光闸调整至 “关闭”状态，完成激光头的预热，待激光显示强度至红色后即可开始对光操作。

（4）对光操作

运用上文 2.4.1 与 2.4.2 中的对光方法完成对光。

2.X 轴对光对比实验

根据统计学中心极限定理设计对比实验，要求 62 位被试人员分为 31 组，每组 2 人分别运用本文 2.4.1 与 2.4.2 中所提出的对光方法完成光路准直，并记录两种方法所需要时长，如表 3-2 所示。

表 3-2 两种不同对光方法所用的时长

	传统的激光干涉仪对光方法	新的激光干涉仪对光方法
平均时长（min）	30.83	12.26

3.2.2 对 X 轴定位精度误差的测量

开始对 X 轴进行螺距误差与反向间隙的测量：在 PC 端软件的相对位置输入机床行程、间隔距离、运行次数、进给率、暂停时间等数据并取消警告选项，点击生成程序，即可自动生成测量所需要的程序，对 X 轴的测量程序见附录三。将此测量程序用 PCMCIA 卡导入机床后运行。

3.2.3 对 X 轴定位精度误差测量结果进行手动及宏程序补偿

结束测量后，得到 X 轴的螺距误差与反向间隙数据，如图 3-4 与表 3-3 所示。将该数据进行手动及宏程序自动补偿。完整程序设计及中英文注释见附录二。

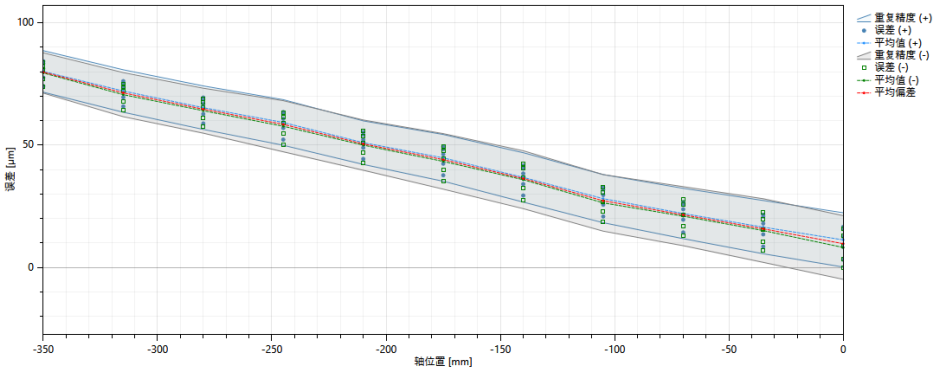

图 3-4 X 轴的螺距误差数据折线图

表 3-3 X 轴的螺距误差与反向间隙数据

反向间隙	-1
螺补点位	螺补数据
0	0
-35	-6
-70	-6
-105	-6
-140	-9
-175	-7
-210	-7
-245	-8
-280	-6
-315	-7
-350	-8

1.手动补偿

在 MDI 模式 system 界面选择“参数”选项，对 3620、3621、3622、3623、3624 及 1851 参数进行设定。参数设定结束后，仍在 MDI 模式 system 界面选择“+”选项中的“螺补”，根据激光测量结果，进行手动输入螺距误差补偿的数据，如表 3-4、3-5 所示。

表 3-4 手动补偿参数设定

参数号	说明	输入数值
3620	参考点的螺距补偿点号	30
3621	负方向最远端的螺距补偿点号	21
3622	正方向最远端的螺距补偿点号	30
3623	螺距补偿倍率	1
3624	螺距补偿点的间隔	35
1851	反向间隙	-1

表 3-5 螺补数值输入

螺补号	输入数值
21	-6
22	-6
23	-6
24	-7
25	-7
26	-7
27	-7
28	-6
29	-7
30	-7

2.宏程序补偿

运用上文 2.5 中提到的宏程序范式，填写相关数据，并通过 PCMCIA 卡导入机床，在机床端运行该程序即可完成参数的自动设定和螺距误差补偿数据的自动输入，X 轴快速补偿宏程序见附录二。

要求 62 位被试人员分为 31 组，每组 2 人分别将上文实验结果进行手动与自动补偿，并记录两种方法所使用的时间，如表 3-6 所示。

表 3-6 两种不同的补偿方法所使用的时长

	手动补偿	宏程序补偿
平均时长（min）	4.96	2.19

3.2.4 对补偿后的 X 轴定位精度误差进行验证

补偿结束后对 X 轴的螺距误差与反向间隙进行验证，其验证结果显示该补偿有效，如图 3-5 所示。

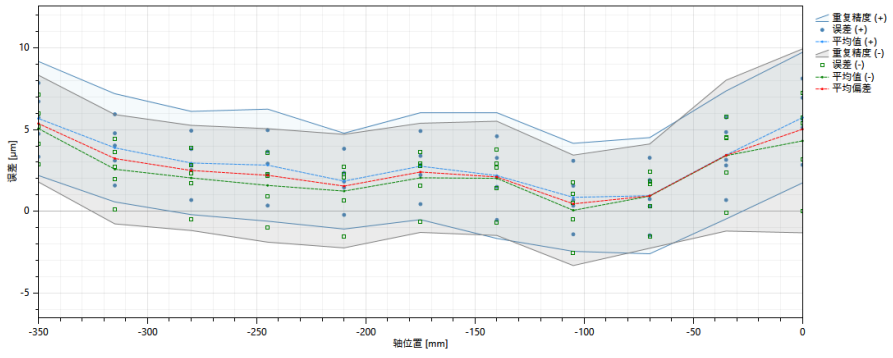

图 3-5 补偿后的 X 轴螺距误差验证结果折线图

3.3 对 Y 轴定位精度误差测量实验

3.3.1 对 Y 轴定位精度误差测量中搭建设备与对光的过程

1. 对 Y 轴进行实验设备的搭建

对 Y 轴进行实验设备的搭建，如图 3-6 所示；Y 轴的搭建过程与 X 轴的搭建过程类似，此处不做赘述。

图 3-6 对 Y 轴螺距误差测量中设备搭建图

2.Y 轴对光对比试验

要求 62 位被试人员分为 31 组，每组 2 人分别运用本文 2.4.1 与 2.4.2 中所提出的对光方法完成光路准直，并记录两种方法所需要时长，如表 3-7 所示。

表 3-7 两种不同对光方法所用的时长

	传统的激光干涉仪对光方法	新的激光干涉仪对光方法
平均时长（min）	24.91	10.04

3.3.2 对 Y 轴定位精度误差的测量

开始对 Y 轴进行螺距误差与反向间隙的测量：在 PC 端软件的相对位置输入机床行程、间隔距离、运行次数、进给率、暂停时间等数据并取消警告选项，点击生成程序，即可自动生成测量所需要的程序，对 Y 轴的测量程序见附录三。将此测量程序用 PCMCIA 卡导入机床后运行。

3.3.3 对 Y 轴定位精度误差测量结果进行手动及宏程序补偿

结束测量后，得到 Y 轴的螺距误差数据折线图与反向间隙数据，如图 3-7 与表 3-8 所示。将该数据进行手动及宏程序自动补偿。完整程序设计及中英文注释见附录二。

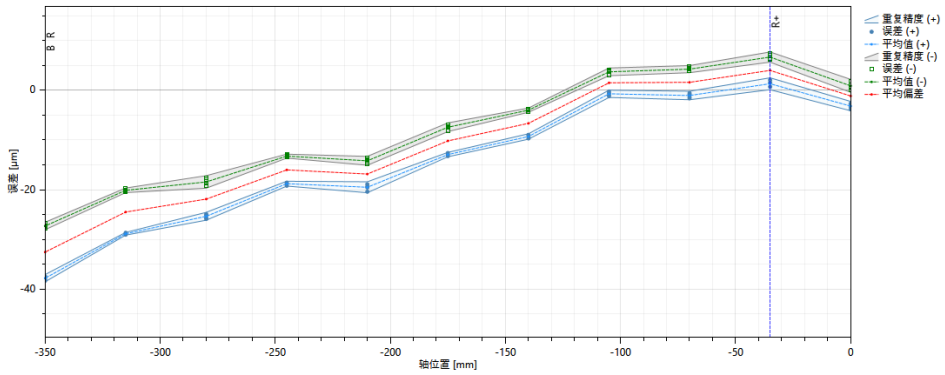

图 3-7 Y 轴的螺距误差数据折线图

表 3-8 Y 轴的螺距误差与反向间隙数据

反向间隙	6
螺补点位	螺补数据
0	0
-35	-5
-70	2
-105	0
-140	9
-175	3
-210	7
-245	-1
-280	6
-315	2
-350	8

1.手动补偿

在 MDI 模式 system 界面选择“参数”选项，对 3620、3621、3622、3623、3624 及 1851 参数进行设定。参数设定结束后，仍在 MDI 模式 system 界面选择“+”选项中的“螺补”，根据参数的设定手动完成对螺距误差的补偿，如表 3-9、3-10 所示。

表 3-9 手动补偿参数设定

参数号	说明	输入数值
3620	参考点的螺距补偿点号	100
3621	负方向最远端的螺距补偿点号	91
3622	正方向最远端的螺距补偿点号	100
3623	螺距补偿倍率	1
3624	螺距补偿点的间隔	35
1851	反向间隙	6

表 3-10 螺补数值输入

螺补号	输入数值
21	-5
22	2
23	0
24	7
25	3
26	7
27	-1
28	6
29	2
30	7

2.宏程序补偿

运用上文 2.5 中提到的宏程序，填写相关数据，并通过 PCMCIA 卡导入机床，在机床端运行该程序即可完成参数的自动设定和螺距误差补偿数据的自动输入，Y 轴快速补偿宏程序见附录二。

要求 62 位被试人员分为 31 组，每组 2 人分别将上文实验结果进行手动与自动补偿，并记录两种方法所使用的时间，如表 3-11 所示。

表 3-11 两种不同的补偿方法所使用的时长

	手动补偿	宏程序补偿
平均时长（min）	5.05	2.36

3.3.4 对补偿后的 Y 轴定位精度误差进行验证

补偿结束后对 Y 轴的螺距误差与反向间隙进行验证，其验证结果显示该补偿有效，如图 3-8 所示。

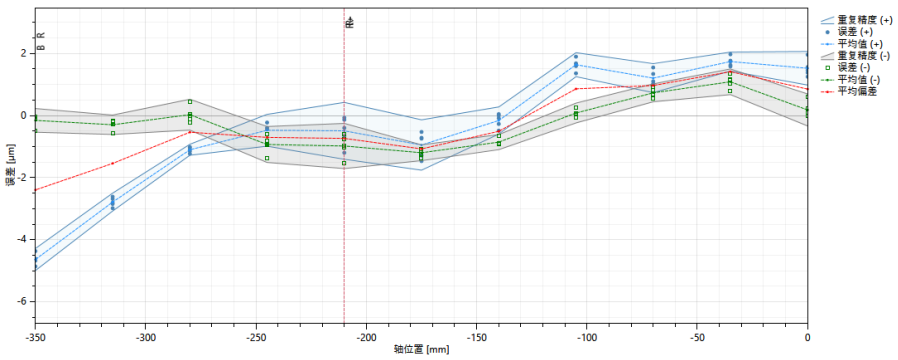

图 3-8 补偿后的 Y 轴螺距误差验证结果折线图

3.4 对 Z 轴定位精度误差测量实验

3.4.1 对 Z 轴定位精度误差测量中搭建设备与对光的过程

1.对 Z 轴进行实验设备的搭建

对 Z 轴进行实验设备的搭建，如图 3-9 所示。

图 3-9 对 Z 轴螺距误差测量中设备搭建图

在设备的搭建与对光中，Z 轴作为垂直轴与水平轴有一定区别：

(1)水平轴的搭建中，将移动反光镜固定至工作台上，将分光镜固定在机床主轴上；而在垂直轴的搭建中，应将移动反光镜固定在机床主轴上，将分光镜固定至工作台上。

(2)在搭建垂直轴的移动反光镜时，应注意移动反光镜的红点应朝向激光头方向。

(3)水平轴的对光中，先准直移动反光镜的光路，后加入分光镜进行对光；而在垂直轴的对光中，先准直分光镜的光路，后加入移动反光镜进行对光。

2.Z 轴对光对比实验

要求 62 位被试人员分为 31 组，每组 2 人分别运用本文 2.4.1 与 2.4.2 中所提出的对光方法完成光路准直，并记录两种方法所需要时长，如表 3-12 所示。

表 3-12 两种不同对光方法所用的时长

	传统的激光干涉仪对光方法	新的激光干涉仪对光方法
平均时长（min）	38.22	15.39

3.4.2 对 Z 轴定位精度误差的测量

开始对 Z 轴进行螺距误差与反向间隙的测量：在 PC 端软件的相对位置输入机床行程、间隔距离、运行次数、进给率、暂停时间等数据并取消警告选项，点击生成程序，

即可自动生成测量所需要的程序，对 Z 轴的测量程序见附录三。将此测量程序用 PCMCIA 卡导入机床后运行。

3.4.3 对 Z 轴定位精度误差测量结果进行手动及宏程序补偿

结束测量后，得到 Z 轴的螺距误差数据折线图与反向间隙数据，如图 3-10 与表 3-13 所示。将该数据进行手动及宏程序自动补偿。完整程序设计及中英文注释见附录二。

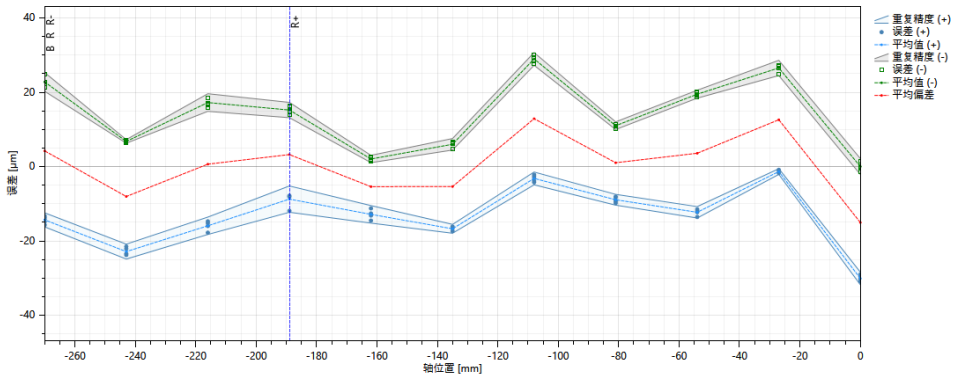

图 3-10 Z 轴的螺距误差数据折线图

表 3-13 Z 轴的螺距误差与反向间隙数据

反向间隙	28
螺补点位	螺补数据
0	0
-27	-28
-54	9
-81	3
-108	-12
-135	18
-162	0
-189	-8
-216	2
-243	9
-270	-12

1.手动补偿

在 MDI 模式 system 界面选择“参数”选项，对 3620、3621、3622、3623、3624 及 1851 参数进行设定。参数设定结束后，仍在 MDI 模式 system 界面选择“+”选项中的“螺补”，根据参数的设定手动完成对螺距误差的补偿，如表 3-14、3-15 所示。

表 3-14 手动补偿参数设定

参数号	说明	输入数值
3620	参考点的螺距补偿点号	80
3621	负方向最远端的螺距补偿点号	71
3622	正方向最远端的螺距补偿点号	80
3623	螺距补偿倍率	4
3624	螺距补偿点的间隔	27
1851	反向间隙	28

表 3-15 螺补数值输入

螺补号	输入数值
21	7
22	1
23	0
24	-2
25	3
26	0
27	-1
28	0
29	1
30	-2

2.宏程序补偿

运用上文 2.5 中提到的宏程序，填写相关数据，并通过 PCMCIA 卡导入机床，在机床端运行该程序即可完成参数的自动设定和螺距误差补偿数据的自动输入，Z 轴快速补偿宏程序见附录二。

要求 62 位被试人员分为 31 组，每组 2 人分别将上文实验结果进行手动与自动补偿，并记录两种方法所使用的时间，如表 3-16 所示。

表 3-16 两种不同的补偿方法所使用的时长

	手动补偿	宏程序补偿
平均时长（min）	5.11	2.16

3.4.4 对补偿后的 Z 轴定位精度误差进行验证

补偿结束后对 Z 轴的螺距误差与反向间隙进行验证，其验证结果显示该补偿有效，如图 3-11 所示。

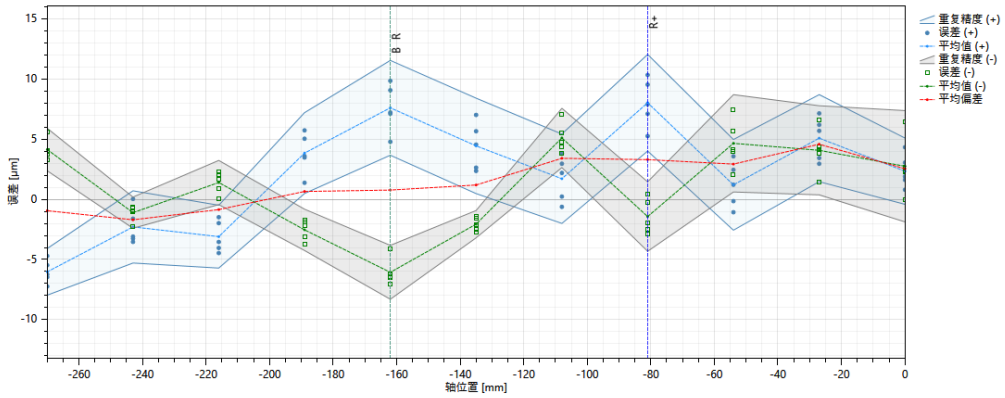

图 3-11 补偿后的 Z 轴螺距误差验证结果折线图

3.5 实验结论

完成了实验准备工作，利用激光干涉仪和加工中心进行实验，分别对 X 轴、Y 轴与 Z 轴进行对光、测量与补偿对比实验，得出实验数据进行比较分析，分别得出新的对光方法时长比传统方法时长在 X 轴上从 30.8 分钟减少到了 12.2 分钟，改善了 60.39%、Y 轴上从 24.9 分钟减少到了 10.0 分钟，改善了 59.84%，Z 轴上从 39.2 分钟减少到了 15.3 分钟，改善了 60.97%，螺距误差宏程序补偿时长比手动补偿时长在 X 轴上从 5.0 分钟减少到了 2.2 分钟，改善了 56.00%、Y 轴上从 5.0 分钟减少到了 2.3 分钟，改善了 54.00%，Z 轴上从 5.1 分钟减少到了 2.0 分钟，改善了 60.78%，如表 3-17 所示。

表 3-17 实验结论

	X 轴	Y 轴	Z 轴
快速对光	60.23%	59.69%	59.73%
快速检测	55.85%	53.27%	57.73%

第四章 结论与展望

4.1 结论

本文以 YL-569 型加工中心（配备 FANUC 0i Mate-MD 数控系统）为研究对象，并查阅了大量参考文献，运用激光干涉仪设计了对 YL-569 型加工中心水平轴与垂直轴的实验方案，确定了本课题的可行性，完成了快速对光与快速补偿实验的设计。本文的具体研究总结如下：

(1)对 YL-569 加工中心进行研究，分析激光干涉仪的构件及使用方法，完成了对激光干涉仪光路准直的理论分析。

(2)激光干涉仪定位精度测量时新旧对光实践方法的对比研究。

(3)设计对螺距误差参数设定与螺补数据补偿的宏程序通用范式。

(4)分别对 X 轴、Y 轴与 Z 轴进行激光干涉仪线性测量对光，得出实验数据进行比较分析，分别得出新的对光方法时长比传统方法时长在 X 轴上改善了 60.23%，在 Y 轴上改善了 59.69%，在 Z 轴上改善了 59.73%。

(5)分别对 X 轴、Y 轴与 Z 轴进行螺距误差补偿对比实验。分别得出宏程序补偿时长比手动补偿时长在 X 轴上改善了 55.85%，在 Y 轴上改善了 53.27%，在 Z 轴上改善了 57.73%。

4.2 展望

激光干涉仪作为测量机床精度的有效工具，尤其在定位精度方面的实用性与精准度更为突出。本文所研究的“新方法”可以有效减少激光干涉仪的线性测量时间，而“新程序”可以有效降低补偿过程中的失误率，同时减少补偿所需要的时间。在上述两个方向中，可有更精深的研究与探讨，本文提出两个对未来的展望：

(1)本文对 YL-569 型加工中心的 X、Y 与 Z 轴进行了螺距误差测量与补偿的实验，该加工中心为平床身，后可通过对激光干涉仪器中角度镜的运用，完成对斜床身机床的快速对光方法研究。

(2)本文仅对机床精度的线性精度进行了测量与补偿，还可以运用激光干涉仪对机床回转轴的角度进行测量与补偿。

参考文献

[1] 王振亚. 省政协委员王辉平： 推动数控机床产业高质量发展[N]. 湖南日报,2022-01-20(008).

[2] 王堃,孙程成,钱锋,王玮,郑巍. 基于激光干涉仪的数控机床定位精度检测与误差补偿方法[J]. 航空制造技术,2010,(21):90-93.

[3] 段伟飞,王海文,张江学. 激光干涉仪在测量数控机床位置精度上的应用[A]. 陕西省机械工程学会. 陕西省机械工程学会 2014 年论文汇编[C].:陕西省机械工程学会数控自动化分会,2022:63-65.

[4] 蒋晓耕,王量,刘畅. 激光干涉仪检测光路的快速校准方法[J]. 机床与液压,2020,48(02):22-27.

[5] 杨晓东.机床数控技术的现状及发展趋势[J]. 湖北农机化,2020,(06):49.

[6] 胡安继,张健,赵东升,贾敏强,王传海. 基于激光干涉法的斜导轨数控机床定位精度检测方法[J]. 计量技术,2020,(01):34-37.

[7] 薛邵文.MVC850B 型立式数控铣床误差分析与补偿试验研究[J]. 机床与液压,2022,50(04):180-186.

[8] 贾平平.激光干涉仪在 PCB 数控机床精度检测中的应用研究[J]. 机床与液压,2018,46(08):129-131.

[9] 蒋幸幸.激光干涉仪在 FANUC 数控机床位置精度检测中的应用[J]. 武汉船舶职业技术学院学报,2019,18(03):127-129+134.

[10] 马磊,钟兴旺,刘玄,任帅. 星间激光干涉仪测距技术发展现状与趋势[J]. 空间电子技术,2018,15(06):1-6.

[11] Jean-Marc Linares, Julien Chaves-Jacob, Heinrich Schwenke,Andrew Longstaff,Simon Fletcher,Jakob Flore,Eckart Uhlmann,Jens Wintering. Impact of measurement procedure when error mapping and compensating a small CNC machine using a multilateration laser interferometer[J]. Precision Engineering,2014,38(3):

[12] Maruyama Daichi,Ibaraki Soichi,Sakata Ryoma. Measurement of Machine Tool Two-Dimensional Error Motions Using Direction-Regulated Laser Interferometers[J]. ijat,2022,16(2).

[13] 赵东升,张健,贾敏强,李维军,管倩倩,朱悦. 测量数控机床定位误差的两种方法之比较[J]. 计量学报,2019,40(S1):33-35.

[14] 郭俊杰,张琳,皮彪. 坐标测量机的空间误差检测及 21 项几何误差分离的方法[J]. 中国机械工程,2002,(13):7-10+3.

[15] John M. Fines,Arvin Agah. Machine tool positioning error compensation using artificial neural networks[J]. Engineering Applications of Artificial Intelligence,2007,21(7).

[16] 机床检验通则 第 2 部分:数控轴线的定位精度和重复定位精度的确定[S].

[17] 全贻智,王晓飞. 用步距规检测数控机床定位精度[J]. 机械工程师,2012,No.251(05):5-6.

[18] 崔剑平,王培林. 浅谈雷尼绍 XL-80 激光干涉仪的对光[J]. 现代制造技术与装备,2015,No.227(04):47-48.

[19] 韩军辉,张秋阳,赵西佳,胡亚杰. 激光干涉仪线性测量的光路准直调整方法[J]. 计量与测试技术,2018,45(10):93-95.

[20] 宋嘎,叶佩青. 基于镜组准直的激光干涉仪快速对光方法研究[J]. 制造技术与机床,2019,No.684(06):150-153.

[21] Mijušković Goran,Krajnik Peter,Kopač Janez. Improvement of positional accuracy of precision micro milling center using pitch error compensation[J]. Tehnički vjesnik,2013,20(4).

致 谢

文至于此，应回顾总结本篇论文的创作历程，笔者的知识储备与分析能力受限，完成本篇论文受到了多方人士的帮助，既是回顾，便也是对多方人士的感恩，所以有致谢一文。

笔者十余年的求学过程中，最能做到“心系学生，服务学生”的便是本文指导教师——左维老师。常言道：“细微之处见真章”，左维老师在学术与生活中的做事哲学，事无巨细、事必躬亲的工作作风，无不令笔者景仰。笔者时常自省，能否追寻其步伐，却也自叹难以望其项背。除左维老师以外，同样要感谢机械工程学院米晶老师、李巍老师对本人论文理论部分的指导与点拨。感谢龚俊杰，王学宽，周源等智能装备应用与维护社团同学对本人论文实验部分的鼎力相助。

文墨将尽，道阻且长。同样值得回顾的是将近四年的求学之路。疫情封锁了学校，但青春仍溢满了我的青葱岁月。感谢校团委刘杰老师、马克思主义学院邢媛院长对本人课外兴趣的栽培与指导，感谢外语学院马力怡老师、马克思主义学院郭丹凤老师、郭文汇老师对本人的帮助与鼓励，感谢艺术学院武麟曾陪伴本人的一岁春秋，感谢陈卓、冯红杉等室友对本人生活上的包容与支持，感谢外语学院仵桐萱、汽轨学院邢子涵、软通学院郭子龙、艺术学院舒雅琪等挚友，与诸君共度锦瑟年华是本人一生幸识。

踔厉奋发，笃定不息。人无法携带太多而过往前行，笔者深知却难抑分别悲伤之情，愿各老师工作顺利，桃李天下；愿同志青年蓬勃向上，勇于攀登，让奋斗成为青春最亮丽的底色！

附录

附录一 中文译文及外文资料

使用方向控制的激光干涉仪测量机床的二维误差运动

Daichi Maruyama, Soichi Ibaraki * and Ryoma Sakata
日本广岛大学先进科学与工程研究生院 1-4-1 Kagamiyama, Higashihiroshima, Hiroshima 739-8511 *日本通讯作者
电子邮件: ibaraki@hiroshima-u.ac.jp

摘要：

机床的定位精度通常随时间变化。在用户现场常以半自动化的方式进行的定期检查，这种方法是可以长期确保足够定位精度的关键。本文提出了一种能测量线性轴的线性定位误差运动的方案，只用激光干涉仪就可以根据一组距离来测量确定一个平面内两个线轴的所有二维（2D）误差运动。与传统的激光干涉仪不同，本文所提出的方案只需要将激光干涉仪安装在一个数值控制的旋转云台上面。它以开环控制的方式根据目标的位置来调节激光束的方向。本文提出了一种算法，除了直接测量两个线性轴的线性定位误差外，还只进行一次跟踪测试来识别两个线性轴的 2D 误差运动。比较了预计误差与直接测量的实验误差以及介绍了不确定性分析。

关键词：机床；几何误差；激光干涉仪；激光跟踪仪

1.简介

机床的定位精度通常会随着时间而变化[1]。环境热变化和机床内部热量，是热影响最典型的原因[2]。摩擦的长期变化，导轨或滚珠丝杠都会改变线性轴的运动误差[3]。通常，在大型机床上，地基水平度或刚度的长期变化会改变机器的水平度，从而改变线性轴的直线度或角度误差[4]。

通常情况下，ISO 230- 1 中描述的精度测试是由机床制造商在机床运送给用户或在用户现场安装时进行的[1]。一旦机床开始在用户现场运行，这些精度测试就很难进行，因为它们需要专用的测量仪器，有经验的测试操作人员，以及大量的停机时间。然而，要完全消除机床几何误差短期或长期的变化是不可能的。他们的定期检查是确保有足够长时间的几何精度的关键。大多数的五轴机床都会进行一种定位精度检测[5]。通常情况下，由机床操作人员在机床工作台上安装一个球体，以半自动的方式用触发式测头测量其中心位置使旋转轴在不同的角度位置进行检测[5]。然后，可以确定旋转轴线性的位置和方向误差，并对其进行相应的数据补偿。如果机床用户定期进行这项测试，可以观察到误差的变化。该测试与 R-测试基本相同，其在热测试中的应用在 ISO 230- 3[8]中有描述[6, 7]。因为这个方案只测量由于主轴与机床工作台的位置不同而产生的相对偏差，它不能单独

测量旋转和线性轴的误差。尤其是大型机床，线性误差可能会因热变化或地基刚度的变化而受到严重影响。最近，某些机床制造商将一种功能商业化，以半自动化的方式在用户现场测量线性误差。例如，日本电产机床公司的大型龙门式加工中心有一个预先校准的球阵列，通常储存在保护盖里，通过使用一个触摸触发探头来测量线性轴的误差运动[9]。大隈公司为大型龙门式机床提供了一种类似的误差校准方式，由机床操作员将一个球阵列或一个正方形放置在机床台上。

球阵的长度决定了其可测量的范围。对于一个较长的轴来说，球阵列装置可能相当昂贵。作为成本较低的替代方案，一些研究人员提出了应用应变片和光纤布拉格光栅传感器来持续预估线性误差[10,11]。他们的预估精度是值得怀疑的，因为他们没有直接测量位置偏差。

对于一个较长的轴，激光干涉仪可能比物理工件更具成本效益，而且其储存部件在测量时间和空间方面更有效率。一个关键问题是，它只能测量单个线性轴的线性定位误差。角度误差的测量往往是令人感兴趣的，因为它们可以显著影响整个工作空间的定位精度，特别是在大型机器上。有各种光学附件可以安装在机床主轴和/或机床工作台上，以便于使用激光干涉仪测量直线度和角度误差[12]。然而，它们的安装和调整无法达到自动化的程度。

本文提出了一种方案，仅用激光干涉仪就可以根据一组距离测量值来估计两个线性轴的线性定位、直线度和（偏）角误差。为了简化测试程序，本研究只针对一个平面上的误差；为了评估三个轴的所有误差，建议该测试必须应用于 XY、YZ 和 ZX 平面。

本方案源于使用跟踪干涉仪（激光干涉仪）进行的多方位测量[13, 14]。在多方位测量中，使用激光干涉仪在不同的四个或更多的位置测量连接到机器主轴上的目标反光镜的距离（对于三维（3D）测量情况）。当只有一个激光干涉仪时，必须在不同的激光干涉仪的位置进行重复相同的测试，这通常需要几个小时。此外，商业激光干涉仪是非常昂贵的。作为一个不太昂贵的替代方案，Ibaraki 等人提出了“开环”激光干涉仪。商业激光干涉仪会自动跟踪反光镜，而“开环”跟踪方案会将激光束方向调节到规定的指令反光镜位置，换句话说，是以“开环”控制的方式进行实验[15-17]。这消除了对自动跟踪机制的需要，使其只需要一个数字控制的控制的旋转云台。

在早期的研究中，它被应用于传统的多方位测量，也就是说，至少需要四次跟踪测试来确定三个线性轴的所有几何误差[15-17]。在多方位测量中，单一的跟踪测试并不能为用户提供有用的信息。当四个测试完成后，所有的误差都可以被计算出来。从某种意义上说，它是一个黑箱测试，只有当所有四个测试都输入时才会输出结果。本文提出的方案由以下测试组成：测试 1 是直接测量两个线性轴的线性定位偏差；测试 2 是通过连续调节激光干涉仪的激光束方向，测量与定位在矩形路径上的反光镜的距离。测试 2 确定了两个线性轴的直线度和角度误差运动。这更接近于传统的单独误差测量，它更适合应用于定期的精度检查。Ibaraki 等人提出了一个类似的方案，但使用的是商用跟踪干涉仪，

而需要机床的旋转轴[18,19]。本文表明，只用一个激光干涉仪就可以测量两个线性轴的所有线性误差。当它的方向可以由一个数控旋转云台来调节时，就可以只用激光干涉仪来测量所有的线性误差。

在 ISO 230-1 中描述的传统精度测试中，每个误差都是用不同的测量仪器在不同的设置中测量的[1]。例如，线性定位误差是用激光干涉仪测量的，直线度误差是用直尺和线性位移传感器测量的。角度误差运动是由自动准直仪测量的。方位误差用一个正方形来测量。本文所提出的方案使用户只需使用一个安装在旋转云台的激光干涉仪就能测量所有的误差。这是一个强大的优势。尽管这种自动安装不在本研究的范围之内，但是如果旋转云台的安装可以是半自动化的。它有可能被应用于自动定期检查精度。

对机床误差的长期监测和自动调整误差补偿可以成为自我优化加工系统的一个重要部分[20]。

Measurement of Machine Tool Two-Dimensional Error Motions Using Direction-Regulated Laser Interferometers

Daichi Maruyama, Soichi Ibaraki†, and Ryoma Sakata

Graduate School of Advanced Science and Engineering, Hiroshima University
1-4-1 Kagamiyama, Higashi-hiroshima, Hiroshima 739-8511, Japan
†Corresponding author, E-mail: ibaraki@hiroshima-u.ac.jp
[Received September 4, 2021; accepted November 19, 2021]

The volumetric accuracy of a machine tool generally changes with time. Its periodic check, performed at a user's site in a semi-automated manner, can be a key to ensure a sufficient volumetric accuracy in the long term. A laser interferometer can only measure the linear positioning error motion of a linear axis. This paper proposes a scheme to identify all the two-dimensional (2D) error motions of two linear axes in a plane based on a set of distance measurements using only a laser interferometer. Unlike conventional tracking interferometers, the proposed scheme requires only a numerically controlled rotary table on which a laser interferometer is mounted. It regulates the laser beam direction based on the command target position in an open-loop control manner. This paper presents an algorithm to identify 2D error motions of two linear axes by performing only a single tracking test, in addition to the direct measurement of linear positioning error motions of two linear axes. The experimental comparison of the estimated error motions with their direct measurements is presented. The uncertainty analysis is also presented.

Keywords: machine tool, geometric errors, laser interferometer, laser tracker

1. Introduction

The volumetric accuracy [1] of a machine tool generally changes with time. Thermal influence, which is typically caused by environmental thermal changes or internal heat sources, is the most typical cause [2]. Long-term changes in friction, lubrication on a guideway, or a ball screw can change linear axis error motions [3]. Typically, on large machine tools, long-term changes in foundation flatness or stiffness can change the machine levelling, and consequently, the straightness or angular error motions of linear axes [4].

Typically, accuracy tests described in, for example, ISO 230-1 [1], are performed by a machine tool builder when a machine tool is shipped to a user or installed at a user's site. Once a machine tool starts operating at a user's site, these accuracy tests are difficult to perform because they require dedicated measuring instruments, experienced test operators, and significant machine downtime. However, it is not possible to completely eliminate the short-term or long-term changes in machine tool geometric errors. Their periodic check is key to ensuring sufficient geometric accuracy in the long term.

A probing-based periodic accuracy check is performed by many five-axis machine tool users [5]. Typically, a precision sphere is installed on a machine table by a machine operator, and a touch-trigger probe measures its center position in a semi-automated manner, with rotary axes indexed at various angular positions [5]. Then, the position and orientation errors of rotary axis average lines can be identified, and their numerical compensation can be updated accordingly. A change in the errors can be observed if a machine tool user performs this test periodically. This test is essentially the same as the R-Test [6, 7], and its application to the thermal test is described in ISO 230-3 [8].

Because this scheme only measures the relative displacement of the spindle to the machine table, it cannot measure rotary and linear axis error motions separately. Linear axis error motions can be significantly influenced by thermal changes or changes in foundation stiffness, especially in larger machines. Recently, certain machine tool builders commercialized a function to measure linear axis error motions at a user's site in a semi-automated manner. For example, a large gantry-type machining center by Nidec Machine Tool Corporation [9] has a pre-calibrated ball array, typically stored in a protective cover, to measure linear axis error motions by using a touch-trigger probe. Okuma Corporation offers a similar probing-based error calibration using a ball array or a square, placed by a machine operator on a machine table, for a large gantry-type machine.

The length of the ball array determines its measurable range. For a longer axis, a ball array artifact can be considerably expensive. As less expensive alternatives, a few researchers have presented the application of strain gauges [10] and fiber Bragg grating sensors [11] to continuously estimate linear axis error motions. Their estimation accuracy is questionable because they do not directly measure the position deviation.

For a longer axis, a laser interferometer may be more cost-effective than physical artifacts and more efficient in terms of the measurement time and space required to store

the instrument. A critical issue is that it can only measure the linear positioning error motion of a single linear axis. The measurement of angular error motions is often of interest because they can significantly influence the volumetric accuracy over the entire workspace, particularly on large machines. Various optical accessories are available to be attached to the machine spindle and/or machine table to measure straightness and angular error motions using a laser interferometer [12]. However, their installation and adjustments cannot be automated.

This paper proposes a scheme to estimate the linear positioning, straightness, and angular (yaw) error motions of two linear axes based on a set of distance measurements using only a laser interferometer. To simplify the test procedure, this study targets only error motions on a plane; to evaluate all the error motions of the three linear axes, the proposed test must be applied to the XY, YZ, and ZX planes.

The present scheme originates from the multilateration measurement using a tracking interferometer (laser tracker) [13, 14]. In the multilateration measurement, the distance to a target retroreflector attached to the machine spindle is measured using a tracking interferometer at four or more different locations (for the three-dimensional (3D) measurement case). When only one tracking interferometer is available, the same test must be repeated with different tracking interferometer positions, which typically takes several hours. Furthermore, commercial tracking interferometers are very expensive. As a less expensive alternative, Ibaraki et al. [15–17] presented the "open-loop" tracking interferometer. Whereas a commercial tracking interferometer automatically follows a retroreflector, the "open-loop" tracking scheme regulates the laser beam direction to the prescribed command retroreflector position, in other words, in an "open-loop" control manner. This eliminates the need for an automated tracking mechanism; it requires only a numerically controlled rotary table.

In earlier studies [15–17], it was applied to the conventional multilateration, that is, at least four tracking tests were required to identify all the 3D error motions of three linear axes. In multilateration, a single tracking test does not provide useful information to a user. When all four tests are completed, all error motions can be calculated. It is, in a sense, a "black-box" test that outputs the results only when all four tests are input. The scheme proposed in this paper consists of the following tests: 1) a direct measurement of the linear positioning deviation of two linear axes, and 2) the distance measurement to the retroreflector, positioned on a rectangular path, by continuously regulating the laser beam direction of a laser interferometer. Test 2 identifies the straightness and angular error motions of the two linear axes. This is closer to conventional separate error motion measurements, and it is more suitable for application to periodic accuracy checks. An analogous scheme was presented by Ibaraki et al. [18, 19], but [18] used a commercial tracking interferometer, whereas [19] required the rotary axis of the machine tool. This paper shows that all the two-dimensional (2D) error motions of two linear axes can be measured using only a laser interferometer when its orientation can be regulated by a numerically controlled rotary table.

Table 1. Two-dimensional error motions of X- and Y-axes. They are identified for all command positions, $k = 1, \ldots, N_x$, $l = 1, \ldots, N_y$.

$E_{XX}(x_k)$	Linear positioning deviation of the X-axis at $x = x_k$
$E_{YX}(x_k)$	Straightness deviation of the X-axis at $x = x_k$
$E_{YY}(y_l)$	Linear positioning deviation of the Y-axis at $y = y_l$
$E_{XY}(y_l)$	Straightness deviation of the Y-axis at $y = y_l$
$E_{CY}(y_l)$	Angular error motion of the Y-axis around the Z-axis at $y = y_l$
$E_{C\perp XY}$	Squareness error of the Y- to X-axis

In conventional accuracy tests described in ISO 230-1 [1], each error motion is measured using a different measuring instrument in a different setup; for example, the linear positioning error motion is measured using a laser interferometer, the straightness error motion is measured by a straightedge and a linear displacement sensor, angular error motions are measured by an autocollimator, and the squareness error is measured using a square. The proposed scheme enables a user to measure all error motions using only a laser interferometer (installed on a rotary table). This is a strong advantage. If the installation of the rotary table on the machine table can be semi-automated, it can be potentially applied to automated periodic accuracy checks for machine tools, although such an automated installation is not within the scope of this study.

The long-term monitoring of machine error motions and automated adaptation of their numerical compensation can be an important part of self-optimizing machining systems [20].

2. Proposed Measurement Test

2.1. Measurement Purpose

The objective of the proposed scheme is to identify all the error motions of two linear axes in a plane, that is, linear positioning, straightness, and angular error motions of each linear axis, as well as the squareness error between them. For example, when the present test was performed on the XY plane, the objective was to identify all the error motions presented in **Table 1**. The error symbols are defined in ISO 230-1 [1].

2.2. Measuring Instrument

The proposed scheme requires a laser interferometer mounted on a rotary table to regulate the direction of the laser beam. The laser interferometer is mounted such that the laser beam approximately intersects with the axis of the rotary table. The rotary table is fixed on a machine table, and a retroreflector is attached to a machine spindle

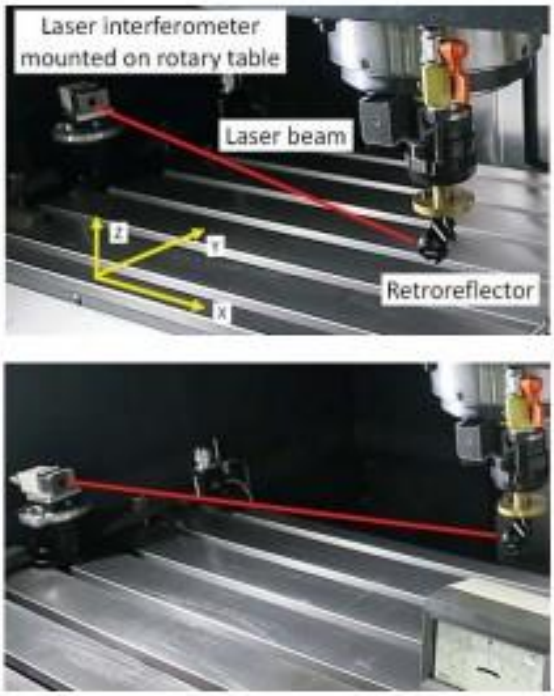

Fig. 1. Proposed test setup. The laser beam is directed to the retroreflector based on its command position.

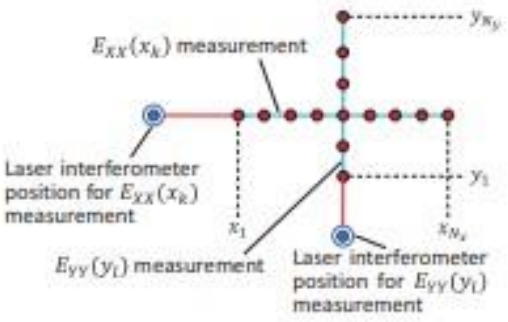

Fig. 2. Direct measurement of the linear positioning error.

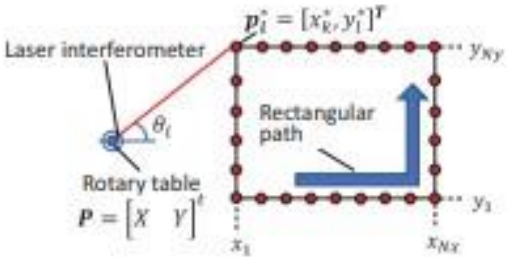

Fig. 3. Tracking measurement of the rectangular command path.

(referred to as the "target" hereafter). A cat's eye retroreflector is typically used, which is a spherical glass of sufficiently high geometric accuracy with its hemispheric surface coated by total-reflection metal-film deposition [21].

2.3. Principle

This device does not have an automatic tracking mechanism such as a laser tracker. Instead, the rotary table is regulated such that the laser beam is directed to the prescribed command position of the target. The angular position of the rotary table, θ_l, can be calculated using Eq. (1) from the target command position, $\boldsymbol{p}_l^* = [x_k^*, y_l^*]^T$ and the position of the axis of the table's rotation, $\boldsymbol{P} = [X, Y]^t$.

$$\theta_l = \arctan\left(\frac{y_l^* - Y}{x_k^* - X}\right). \quad \cdots\cdots\cdots \quad (1)$$

Figure 1 demonstrates a test setup. As the target is at an arbitrary command position, the laser beam is directed to it by the rotary table.

Clearly, the laser beam is not directed exactly to the retroreflector center because of an error in the target position. The angular positioning error of the rotary table also contributes to the laser beam direction error. The position of the rotary table, $\boldsymbol{P}$, must be roughly estimated in advance (see Remark b) in Section 2.4).

The estimation error also contributes to the laser beam direction error. However, they impose only the "cosine error" on the laser displacement. In the application to machine tool calibration, it is reasonable to assume that the positioning error of the machine is sufficiently small to make its "cosine error" negligibly small. This influence on the measurement uncertainty will be further studied in Section 5.

2.4. Procedure

This paper proposes the following procedure:

1) Install the rotary table, on which the laser interferometer is mounted, on the machine table, and attach the target to the spindle.
2) Set the zero angular position of the rotary table such that the laser beam is roughly aligned to the X-axis of the machine.
3) Roughly estimate the position of the axis of the table's rotation, $\boldsymbol{P} = [X, Y]^t$. See Remark b) below.
4) Measure the linear positioning deviation in the X- and Y-axes. This can be measured by positioning the target in the X (or Y) direction at the same Y (or X) position as the rotary table (see **Fig. 2**). The measured laser displacements in the X- and Y-directions are denoted by $d_{k1} \in \mathbb{R}$ for the command position x_k $(k = 1, \ldots, N_x)$ and d_{l2} for the command position y_l $(l = 1, \ldots, N_Y)$, respectively.
5) Position the target along a rectangular path (**Fig. 3**) in the range $x_k = x_1, \ldots, x_{N_x}$ and $y_l = y_1, \ldots, y_{N_y}$, and measure the distance (displacement) to the target by

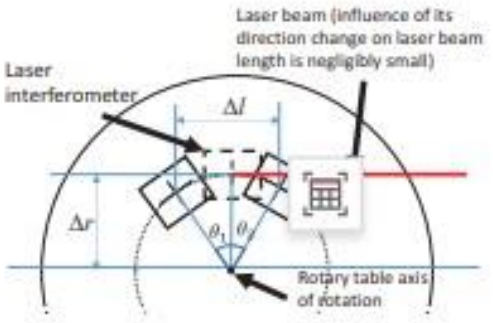

Fig. 4. Influence of the misalignment of the laser interferometer to the axis of the rotary table on the laser beam length.

controlling the laser beam at the angle as given in Eq. (1). When the commanded position of the target is $\boldsymbol{p}_i^* = [x_k^*, y_l^*]^t$ $(i = 1, \ldots, 2(N_x + N_y) - 4)$, the measured laser displacement is denoted by $d_{i3} \in \mathbb{R}$.

Remarks

a) Alignment of the laser beam to the axis of the rotary table: In the proposed scheme, the laser interferometer is mounted on the rotary table such that the laser beam approximately intersects with the axis of the rotary table, $\boldsymbol{P}$. The misalignment, Δr in **Fig. 4**, can be minimized by the following procedure. First, direct the laser beam to the retroreflector such that the distance to it can be measured. Then, rotate the rotary table within a small range, θ_1 and θ_2 in **Fig. 4**, where the distance is measurable. Adjust the laser interferometer position such that the variation in the measured distance, Δl in **Fig. 4**, is minimized.

b) Rough estimation of the position of the rotary table: The following methods can be used to estimate the position of the axis of the table rotation, $\boldsymbol{P}$. First, position the retroreflector at the n-th position, $\boldsymbol{p}_n^v = [p_{nx} \quad p_{ny}]^t$ $(n = 1, \ldots, N)$. Manually direct the laser beam to the retroreflector. Denote the direction of the laser beam by the direction vector $\boldsymbol{l}_n = [l_{nx} \quad l_{ny}]^t$ (with $\|\boldsymbol{l}_n\| = 1$) from the angular position of the rotating table. Define a line that passes $\boldsymbol{p}_n^v$ in direction l_n (see **Fig. 5**). The closest point, $\boldsymbol{q}_n^v$ in **Fig. 5**, on this line to point $\boldsymbol{P} = [X, Y]^t$ is expressed as follows:

$$\boldsymbol{q}_n^v = \boldsymbol{p}_n^v + t_n^* \boldsymbol{l}_n, \quad \ldots\ldots\ldots\ldots \quad (2)$$

where t_n^* represents the length of the projection of the vector, $\boldsymbol{P} - \boldsymbol{p}_n^v$, to this line and is expressed as follows:

$$t_n^* = l_{nx}(X - p_{nx}) + l_{ny}(Y - p_{ny}). \quad \ldots \quad (3)$$

Thus, the distance from $\boldsymbol{P}$ to the line, b_n in **Fig. 5**, is formulated as follows:

$$b_n = \left\| \boldsymbol{P} - (\boldsymbol{p}_n^v + t_n^* \boldsymbol{l}_n) \right\|. \quad \ldots\ldots\ldots \quad (4)$$

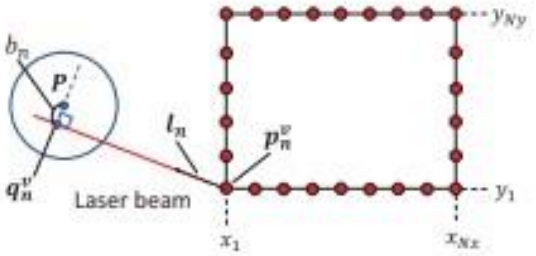

Fig. 5. Identification method for the axis of the table's rotation, $\boldsymbol{P}$.

Determine $\boldsymbol{l}_n$ for every target position $\boldsymbol{p}_n^v$ with $n = 1, \ldots, N$. For example, the target is positioned at four vertices of the command path ($N = 4$, see **Fig. 5**). Then, the rotary table position, $\boldsymbol{P}$, can be estimated by solving

$$\min_{\boldsymbol{P}} \sum_n {b_n}^2. \quad \ldots\ldots\ldots\ldots \quad (5)$$

This only provides a rough estimate for the axis of the rotary table, $\boldsymbol{P}$, because the laser beam directions, $\boldsymbol{l}_n$, can contain a significant error.

3. Algorithm to Estimate Linear Axis Error Motions

In addition to the error motion parameters shown in **Table 1**, the rotary table position, $\boldsymbol{P} \in \mathbb{R}^2$, and the dead path lengths of the laser interferometer, $\boldsymbol{d_{0j}} = [d_{01}, d_{02}, d_{03}]^t$ ($j = 1$: direct measurement of E_{XX}, $j = 2$: direct measurement of E_{YY}, $j = 3$: tracking measurement) are identified. The dead path length is defined as the distance between the laser interferometer and the initial position of the target. This must be identified because a laser interferometer only measures the displacement from the dead path length.

The parameters to be identified are combined into a single vector $\in \mathbb{R}^{2\times N_x+3\times N_y+1+3+2}$.

$$\boldsymbol{X} = \Big[\left\{ E_{XX}(x_k), E_{YX}(x_k) \right\}_{k=1,\ldots,N_x}, \left\{ E_{YY}(y_l), E_{XY}(y_l), E_{CY}(y_l) \right\}_{l=1,\ldots,N_y}, E_{C(0X)Y}, \boldsymbol{d_{0j}}, \boldsymbol{P} \Big]^T \quad \ldots\ldots\ldots\ldots \quad (6)$$

This study considers the machine configuration shown in **Fig. 6** as an example. When the retroreflector attached to the spindle is positioned at the command position $\boldsymbol{p}_i^* = [x_k^*, y_l^*]^t$, its 2D positioning error is modelled as follows, according to the well-established machine kinematic modeling theory [5]:

$$\boldsymbol{\Delta p_i} = \begin{bmatrix} E_{XX}(x_k) + E_{XY}(y_l) \\ E_{YX}(x_k) + E_{YY}(y_l) + \left(E_{C(0X)Y} + E_{CY}(y_l) \right) x_k \end{bmatrix}. \quad (7)$$

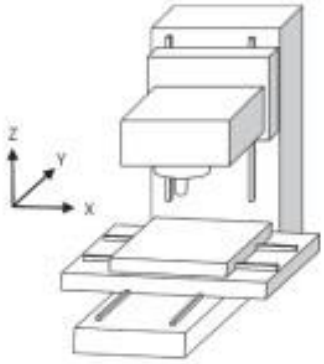

Fig. 6. Machine tool configuration.

Using Eq. (6), Eq. (7) can be rewritten as follows:

$$\begin{bmatrix} \Delta \boldsymbol{p}_i \\ \boldsymbol{d}_{0j} \\ \boldsymbol{P} \end{bmatrix} = \begin{bmatrix} C_{kinematic}(\boldsymbol{p}_i^*) & 0 \\ 0 & I \end{bmatrix} \boldsymbol{X}, \quad \ldots\ldots (8)$$

where $C_{kinematic}(\boldsymbol{p}_i^*) \in \mathbb{R}^{2\times(2N_x+3N_y+1)}$ represents a constant matrix constructed using Eq. (7). Then, $\boldsymbol{X}$ in Eq. (8) can be identified by solving the following problem.

$$\min_{\boldsymbol{X}} \sum_j \sum_i \left(f_i \left(\begin{bmatrix} \Delta \boldsymbol{p}_i \\ \boldsymbol{d}_{0j} \\ \boldsymbol{P} \end{bmatrix} \right) - \boldsymbol{d}_{ij} \right)^2, \quad \ldots\ldots (9)$$

where function f_i represents the distance between the target position, $\boldsymbol{p}_i = \boldsymbol{p}_i^* + \Delta \boldsymbol{p}_i$, and the rotary table position, $\boldsymbol{P}$, and is defined as follows:

$$f_i \left(\begin{bmatrix} \Delta \boldsymbol{p}_i \\ \boldsymbol{d}_{0j} \\ \boldsymbol{P} \end{bmatrix} \right) = \| \boldsymbol{p}_i - \boldsymbol{P} \| - \boldsymbol{d}_{0j}. \quad \ldots\ldots (10)$$

Furthermore, the following constraints are required to define the coordinate system and error motions uniquely.

$$\begin{cases} E_{XX}(x_1) = E_{YX}(x_1) = E_{YY}(y_1) = E_{XY}(y_1) \\ \qquad\qquad = E_{CY}(y_1) = 0 \\ E_{YX}(x_{N_x}) = E_{XY}(y_{N_y}) = 0 \end{cases}. \quad (11)$$

Variable $\boldsymbol{X}$ can be identified by solving Eq. (9) from the measured laser displacements, $\boldsymbol{d}_{ij}$, by applying, for example, the Newton method.

4. Case Study

4.1. Measuring Instrument

Figure 7 depicts the developed prototype. **Fig. 8** shows the configuration. The laser interferometer was mounted on the rotary table via a screw-driven stage that is used to adjust the laser beam's position such that it passes through the axis of rotation of the rotary table (see Remark a) in Section 2.4). A cat's eye retroreflector by Etalon AG was attached to the machine spindle as the target.

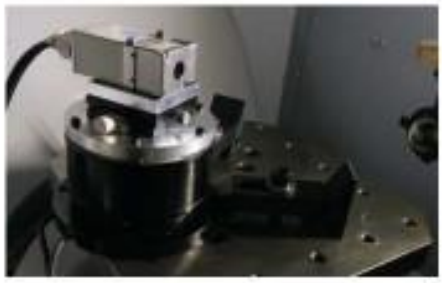

Fig. 7. Prototype measuring instrument.

The major specifications of the rotary table, laser interferometer, and cat's eye retroreflector are listed in **Tables 2**, **3**, and **4**, respectively.

4.2. Experimental Setup

Figure 9 demonstrates the experimental setup. **Fig. 10** shows the rotary table position, $\boldsymbol{P}$, estimated using the scheme presented in Remark b) in Section 2.4 and the command trajectory of the retroreflector. The linear positioning deviation of the X-axis, d_{k1}, and the square path were measured using the rotary table at $\boldsymbol{P}$. The linear positioning deviation of the Y-axis, d_{l2}, was measured for different rotary table positions. For the rectangular path, to synchronize the machine tool and the rotary table, the movement of the machine tool from the initial position was detected using a digital indicator (see **Fig. 8**) that starts the rotation of the rotary table. The time constant in the acceleration/deceleration of the rotary table was adjusted such that it was synchronized with the machine tool. Three measurements were taken, and the average laser displacement was used for identification.

4.3. Estimated Error Motions

Figure 11 shows the measured linear positioning deviations of the (a) X-axis, $E_{XX}(x_k)$, and (b) Y-axis, $E_{YY}(y_l)$. **Fig. 12(a)** displays the measured laser displacement profile obtained by the tracking measurement, d_{i3} $(i = 1, \ldots, 2(N_x + N_y) - 4)$, for the rectangular command path, $\boldsymbol{p}_i^*$, as shown in **Fig. 10**. **Fig. 12(b)** shows the difference in the measured laser displacement profile, d_{i3}, to its nominal length, $\| \boldsymbol{p}_i^* - \boldsymbol{P} \|$, when assuming no error motion of the X- and Y-axes. The algorithm proposed in Section 3 identifies $\boldsymbol{X}$ such that this difference is minimized. The measurements were performed three times, and only the average values are shown in **Figs. 11** and **12**.

Figure 13 depicts error motions estimated using the proposed algorithm: (a) the straightness deviation of the X-axis, $E_{YX}(x_k)$, (b) the straightness deviation of the Y-axis, $E_{XY}(y_l)$, and (c) the angular (yaw) deviation of the Y-axis around the Z-axis, $E_{CY}(y_l)$. Combining the identified error motions shown in **Fig. 13** using the kinematic

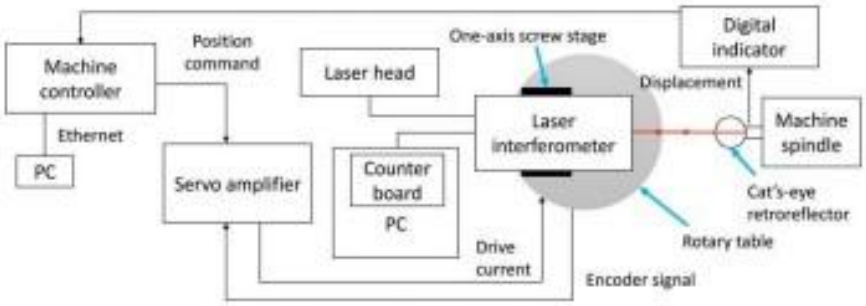

Fig. 8. Configuration of the measuring instrument.

Table 2. Major specifications of the rotary table (SGM7D-03H7C42 by Yaskawa Electric Co., Ltd.).

Drive system	Direct drive
Angle of rotation	360° endless
Maximum torque	4 N·m
Maximum rotation speed	150 min^{-1}
Encoder resolution	16777216 pulse/rev
Positioning accuracy	±15 arcsec
Positioning repeatability	±1.3 arcsec
Weight	3 kg
Height	77 ± 0.5 mm
Table size	ϕ116 mm

Table 3. Major specifications of the laser interferometer (Distax L-IM-300A by Tokyo Seimitsu Co., Ltd.).

Laser	He-Ne laser
Wavelength	632.991832 nm
Range of measurement	10 m
Resolution	$\lambda/64$ (0.01 μm)
Maximum response speed	630 s^{-1}
Measurement accuracy	$\pm(\|L\| \times 10^{-7} + 0.005 \times 10^{-6})$ m where L is the measurement length

Table 4. Major specifications of the cat's eye retroreflector (by Etalon AG).

Viewing angle	±80°
Optical form deviation	< 0.2 μm

model Eq. (7), the 2D positioning error can be predicted at an arbitrary command position. **Fig. 14** shows the estimated 2D positioning error profiles for the command path shown in **Fig. 10**.

4.4. Validation of Estimated Error Motions

The validity of a part of the estimated error motions was experimentally investigated by comparison with other direct measurements. The measurements were performed

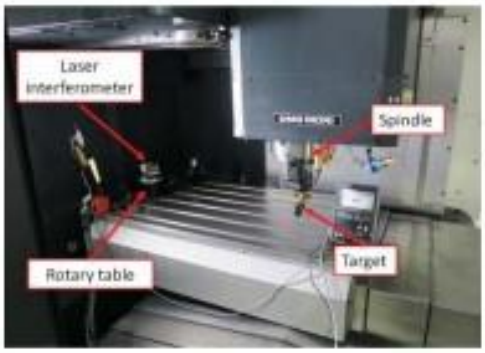

Fig. 9. Experimental setup.

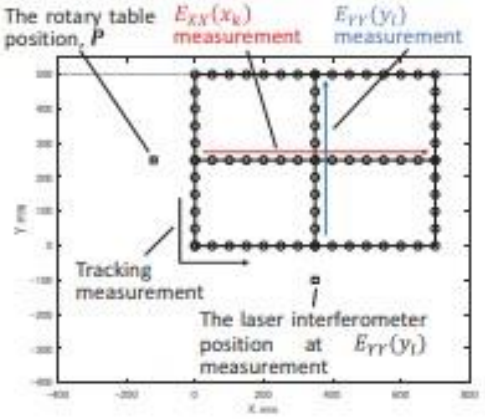

Fig. 10. Command positions of the spindle's reference point and the rotary table positions.

using a laser interferometer, XL-80 by Renishaw Co., Ltd. This instrument can measure linear positioning, straightness, and angular error motions using various optical accessories. Measurements were taken three times each, and the average of these values was used for comparison.

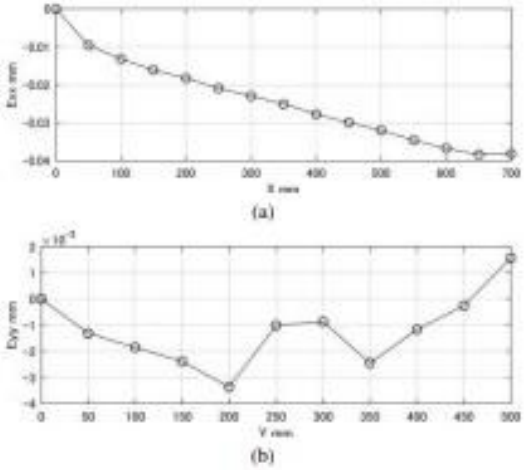

Fig. 11. Measured linear positioning deviation of the (a) X-axis, $E_{XX}(x_k)$, and (b) Y-axis, $E_{YY}(y_l)$. The horizontal axis represents the command X- (Y-)axis positions, x_k^* (y_l^*).

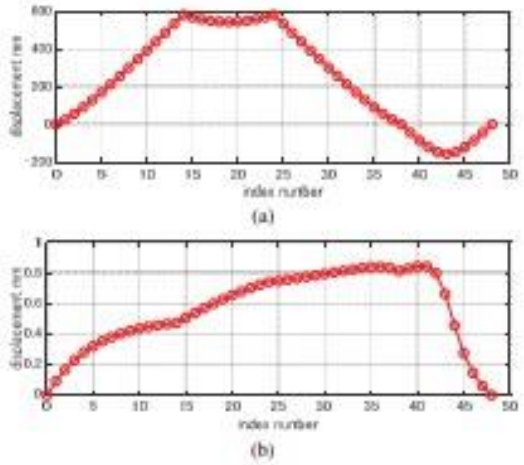

Fig. 12. (a) Measured laser displacement by the proposed "open-loop" tracking interferometer measurement, d_{Oi} ($i = 1, \ldots, 2(N_x + N_y) - 4$). (b) The difference in the measured laser displacement profile (a) to its nominal length, $\|\boldsymbol{p}_i^* - \boldsymbol{P}\|$, assuming no geometric error of the machine tool.

Figure 15 compares the measured error motions with the estimates by the proposed scheme. The straightness deviation of the X-axis, estimated using the proposed scheme, that is, the difference between the maximum and the minimum of $E_{YX}(x_k)$, was approximately 5 μm (measurement distance 700 mm), and the straightness error of the Y-axis, $E_{XY}(y_l)$, was approximately 5 μm (measurement distance 500 mm), whereas the measured straightness deviation of the X- and Y-axes were 2 μm and 1 μm, respectively. In both cases, the values identified by the proposed scheme were larger. This difference might be

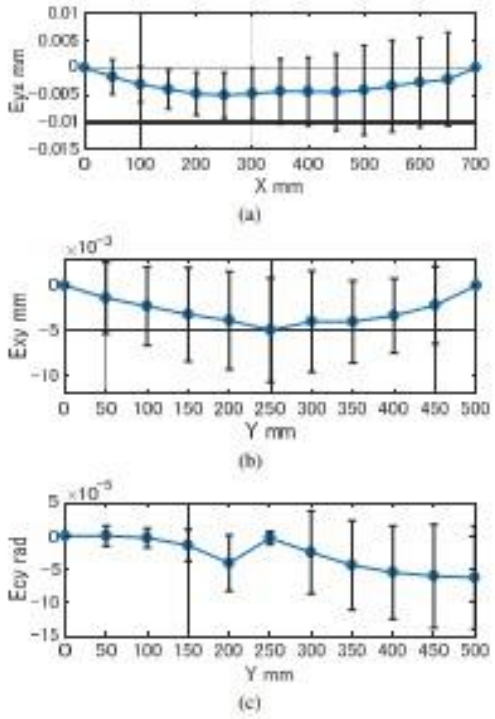

Fig. 13. Estimated linear axis error motions by the proposed algorithm. (a) The straightness deviation of the X-axis, $E_{YX}(x_k)$, (b) the straightness deviation of the Y-axis, $E_{XY}(y_l)$, and (c) the yaw error motion of the Y-axis around the Z-axis, $E_{CY}(y_l)$. Vertical error bars represent the uncertainty ($k = 2$) (see Section 5.3).

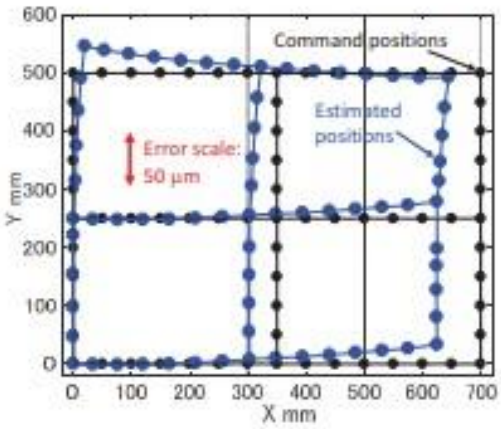

Fig. 14. Estimated spindle reference point positions by the proposed scheme. The error between estimated and command positions is magnified 2000 times (see "Error scale").

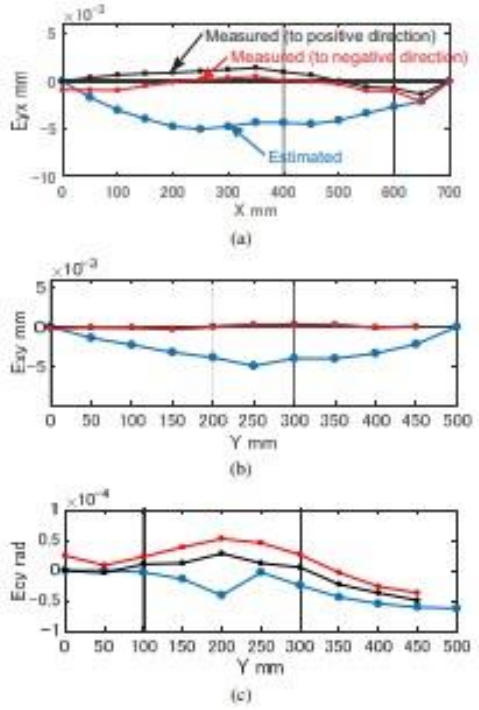

Fig. 15. Comparison of the measured error motions with their estimates by the proposed scheme. (a) The straightness deviation of the X-axis, $E_{YX}(x_i)$, (b) the straightness deviation of the Y-axis, $E_{XY}(y_i)$, and (c) the yaw error motion of the Y-axis around the Z-axis, $E_{CY}(y_i)$.

caused by the uncertainty in the distance measurement of the laser interferometer. This is further discussed in Section 5. Furthermore, it may be attributable to the difference in the measured positions in the two tests. In the straightness measurement using a laser interferometer, the displacement of the straightness reflector installed on the machine table was directly measured. In the proposed test, the displacement of the laser interferometer determines the measured laser displacement, which is converted to straightness error motion at $X = 0$ (or $Y = 0$). For example, a large machine tool table may elastically deform because of its weight when it is mounted on two linear axes (see **Fig. 6**). This may cause different straightness error motions measured at different positions.

5. Uncertainty Analysis

5.1. Objective

The proposed test procedure has uncertainty contributors that are, in principle, negligible in conventional multilateration. Unlike an automated tracking interferometer, the laser beam is directed to the command target position, as shown in Eq. (1). When there exists a positioning error of the machine tool, the laser beam is not directed exactly to the center of the retroreflector. To validate the proposed scheme, it is crucial to show that such an influence does not have a significant influence on the overall measurement uncertainty when the machine tool, as well as the measuring instrument and its setup, has a "typical" accuracy. The uncertainty analysis presented in this section is analogous to those presented in the authors' previous works [15–17, 19].

Table 5. Uncertainty budget ($k = 2$) for laser displacement when the target is at $\boldsymbol{p}^*_{25} = [700, 500]$ mm.

Symbol		Contributor	Value
U	Extended uncertainty containing u_1, u_2, and u_3 ($k = 2$)		2.70 μm
u_1	Uncertainty in the distance measurement by the laser interferometer ($k = 1$)		1.30 μm
	u_{11}	Uncertainty in laser interferometry	0.02 μm
	u_{12}	Uncertainty owing to the wavelength correction	0.72 μm
	u_{13}	Uncertainty owing to changes in environment	1.08 μm
u_2	Uncertainty owing to machine positioning repeatability ($k = 1$)		0.4 μm
u_3	Uncertainty owing to the laser beam orientation error ($k = 1$)		0.1 μm
	u_{31}	Uncertainty in the rotary table zero angular position	$3.5 * 10^{-4}$ rad
	u_{32}	Angular positioning error of the rotary table	$0.18 * 10^{-4}$ rad
	u_{33}	Error in the estimated retroreflector position	$9.0 * 10^{-4}$ rad
	u_{34}	Uncertainty owing to the machine tool positioning error	$0.34 * 10^{-4}$ rad

5.2. Uncertainty Budget for Laser Displacements

Table 5 presents the uncertainty budget ($k = 2$) for the laser displacement when the target was at $\boldsymbol{p}^*_{25} = [700, 500]$ mm. The uncertainty depends on the laser beam length, and this point is presented as an example.

The uncertainty in the distance measurement by the laser interferometer, u_1, was assessed by the uncertainty in the wavelength, u_{11}, provided by the manufacturer ($u_1 = |L| \cdot 10^{-7} + 0.005 \cdot 10^{-6}$, where L is the measured length in meters) and the uncertainty in temperature, humidity, and air pressure measurements (u_{12} and u_{13}). The uncertainty owing to machine positioning repeatability, u_2, was experimentally assessed by repeating positioning experiments. The influence of the angular positioning error of the rotary table on the laser distance, u_{32}, is the "cosine error" and was assessed based on the catalog performance of the rotary table. Other contributors to the uncertainty in the laser beam direction (u_{31}, u_{33}, and u_{34}) also result in the "cosine error" on the laser length.

5.3. Uncertainty in Estimated Error Motions

The uncertainty in the laser displacement propagates into the uncertainty in the estimated error motions. This relationship cannot be analytically formulated because it involves the numerical optimization in Eq. (9). In such a case, a Monte Carlo simulation can be applied for uncertainty evaluation [22].

The vertical error bars in **Fig. 13** show the extended uncertainty ($k = 2$) for each error motion parameter in Eq. (5). They were assessed by running the Monte Carlo simulation 1,000 times.

Table 5 shows that the uncertainty in the distance measurement by the laser interferometer, u_1, is a major uncertainty contributor, whereas the contribution of laser beam orientation error, u_3, is minor. This indicates that the overall uncertainty of the present scheme does not significantly differ from the multilateration by using a commercial automated tracking interferometer. **Fig. 12** indicates that the tested error motions of the machine tool may not be significantly larger than the uncertainty in the laser interferometer measurement.

6. Conclusion

The contributions of this paper can be summarized as follows:

- A novel scheme is proposed to identify all the error motions of two linear axes in a plane using a set of distance measurements using only a laser interferometer. In the tracking test, the direction of the laser interferometer was regulated by a rotary table toward the command target position. The linear positioning deviations of each axis were measured separately.

- In the experiment, the error motions identified by the proposed method were compared with the directly measured straightness deviation of the X- and Y-axes and the angular error motion of the Y-axis around the Z-axis.

- The effect of various uncertainty contributors, with a particular focus on the laser beam orientation error, which is in principle negligible in conventional multilateration, on the uncertainty of the identification of error motions was analyzed. Notably, the uncertainty in the laser measurement was the major contributor, and the contribution of the laser beam orientation error was minor.

References:

[1] ISO 230-1:2012, "Test code for machine tools – Part 1: Geometric accuracy of machines operating under no-load or quasi-static conditions," 2012.

[2] J. Mayr, J. Jedrzejewski, E. Uhlmann, M. A. Donmez, W. Knapp, F. Hartig, K. Wendt, T. Moriwaki, P. Shore, E. Schmitt, C. Brecher, T. Wurz, and K. Wegener, "Thermal issues in machine tools," CIRP Annals, Vol.61, No.2, pp. 771-791, 2012.

[3] M. Reuss, A. Dadalau, and A. Verl, "Friction Variances of Linear Machine Tool Axes," Procedia CIRP, Vol.4, pp. 115-119, 2012.

[4] K. Mori, D. Kono, and A. Matsubara, "A robust level error estimation method for machine tool installation," Precision Engineering, Vol.58, pp. 70-76, 2019.

[5] S. Ibaraki and W. Knapp, "Indirect Measurement of Volumetric Accuracy for Three-Axis and Five-Axis Machine Tools: A Review," Int. J. Automation Technol., Vol.6, No.2, pp. 110-124, doi: 10.20965/ijat.2012.p0110, 2012.

[6] S. Weikert, "R-Test, a New Device for Accuracy Measurements on Five Axis Machine Tools," CIRP Annals, Vol.53, No.1, pp. 429-432, 2004.

[7] S. Ibaraki, C. Oyama, and H. Otsubo, "Construction of an error map of rotary axes on a five-axis machining center by static R-test," Int. J. of Machine Tools and Manufacture, Vol.51, No.3, pp. 190-200, 2011.

[8] ISO 230-3:2020, "Test code for machine tools – Part 3: Determination of thermal effects," 2020.

[9] K. Iwata, K. Fujimoto, and S. Nakamura, "Improvement and stabilization of spatial accuracy of whole processing area by three-dimensional spatial error correction system in milling machine," Mitsubishi Heavy Industries Technical Review, Vol.57, No.3, pp. 1-3, 2020.

[10] Y.-Q. Wang, J.-K. Wu, H.-B. Liu, K. Kang, and K. Liu, "Geometric accuracy long-term continuous monitoring using strain gauges for CNC machine tools," Int. J. of Advanced Manufacturing Technology, Vol.98, pp. 1145-1153, 2018.

[11] F. Aggogeri, A. Borboni, R. Faglia, A. Merlo, and N. Pellegrini, "A Kinematic Model to Compensate the Structural Deformations in Machine Tools Using Fiber Bragg Grating (FBG) Sensors," Applied Sciences, Vol.7, No.2, Article No.114, 2017.

[12] ISO/TR 230-11:2018, "Test code for machine tools – Part 11: Measuring instruments suitable for machine tool geometry tests," 2018.

[13] H. Schwenke, M. Franke, J. Hannaford, and H. Kunzmann, "Error mapping of CMMs and machine tools by a single tracking interferometer," CIRP Annals, Vol.54, No.1, pp. 475-478, 2005.

[14] S. Ibaraki, T. Kudo, T. Yano, T. Takatsuji, S. Osawa, and O. Sato, "Estimation of three-dimensional volumetric errors of machining centers by a tracking interferometer," Precision Engineering, Vol.39, pp. 179-186, 2014.

[15] S. Ibaraki, G. Sato, and K. Takeuchi, "'Open-loop' tracking interferometer for machine tool volumetric error measurement – Two-dimensional case," Precision Engineering, Vol.38, No.3, pp. 666-672, 2014.

[16] S. Ibaraki, K. Nagae, and G. Sato, "Proposal of 'open-loop' tracking interferometer for machine tool volumetric error measurement," CIRP Annals, Vol.63, No.1, pp. 501-503, 2014.

[17] S. Ibaraki and K. Tsuboi, "'Open-loop' tracking interferometer measurement using rotary axes of a five-axis machine tool," IEEE/ASME Trans. on Mechatronics, Vol.22, No.5, pp. 2342-2350, 2017.

[18] S. Ibaraki, P. Blaser, M. Shimoike, N. Takayama, M. Nakamuro, and Y. Ido, "Measurement of thermal influence on a two-dimensional motion trajectory using a tracking interferometer," CIRP Annals, Vol.65, No.1, pp. 483-486, 2016.

[19] S. Ibaraki and M. Haruya, "A novel scheme to measure 2D error motions of linear axes by regulating the direction of a laser interferometer," Precision Engineering, Vol.67, pp. 152-159, 2021.

[20] H.-C. Möhring, P. Wiederkehr, K. Erkorkmaz, and Y. Kakinuma, "Self-optimizing machining systems," CIRP Annals, Vol.69, No.2, pp. 740-763, 2020.

[21] T. Takatsuji, M. Goto, S. Osawa, R. Yin, and T. Kurosawa, "Whole-viewing-angle cat's-eye retroreflector as a target of laser trackers," Measurement Science and Technology, Vol.10, No.7, pp. 87-90, 1999.

[22] JCGM 101:2008, "Evaluation of measurement data – Supplement 1 to the Guide to the expression of uncertainty in measurement – Propagation of distributions using a Monte Carlo method," 2008.

Name:
Daichi Maruyama

Affiliation:
Graduate School of Advanced Science and Engineering, Hiroshima University

Address:
1-4-1 Kagamiyama, Higashi-hiroshima, Hiroshima 739-8511, Japan

Brief Biographical History:
2018- Undergraduate Student, Hiroshima University
2022- Master Course Student, Hiroshima University

Name:
Soichi Ibaraki

Affiliation:
Professor, Graduate School of Advanced Science and Engineering, Hiroshima University

Address:
1-4-1 Kagamiyama, Higashi-hiroshima, Hiroshima 739-8511, Japan

Brief Biographical History:
2001- Research Associate, Kyoto University
2006- Associate Professor, Kyoto University
2016- Professor, Hiroshima University

Main Works:
• S. Ibaraki, N. A. Theissen, A. Archenti, and M. M. Alam, "Evaluation of Kinematic and Compliance Calibration of Serial Articulated Industrial Manipulators," Int. J. Automation Technol., Vol.15, No.5, pp. 567-580, 2021.
• S. Ibaraki and W. Knapp, "Indirect Measurement of Volumetric Accuracy for Three-Axis and Five-Axis Machine Tools: A Review," Int. J. Automation Technol., Vol.6, No.2, pp. 110-124, 2012.

Membership in Academic Societies:
• Japan Society for Precision Engineering (JSPE)
• Japan Society of Mechanical Engineers (JSME)
• American Society of Mechanical Engineers (ASME)

Name:
Ryoma Sakata

Affiliation:
Graduate School of Engineering, Hiroshima University

Address:
1-4-1 Kagamiyama, Higashi-hiroshima, Hiroshima 739-8511, Japan

Brief Biographical History:
2020- Advanced Technology Development Control Department, DMG Mori Co., Ltd.

附录二 螺距误差补偿参数快速输入的宏程序

X 轴补偿宏程序：

%

O8010；

G10L52；（设定参数输入方式）

#1=1（选择轴为 X 轴）(X axis)

N11502R00001100；（执行宏程序调用和可编程参数输入高速执行）

N3620P#1R30；（X 轴参考点的螺距补偿点号为 30）(NO. of PITCH for X)

N3621P#1R21；（X 轴负方向最远端的螺距补偿点号为 30）(NO. of PITCH for -X)

N3622P#1R30；（X 轴正方向最远端的螺距补偿点号为 21）(NO. of PITCH for +X)

N3623P#1R1；（X 轴螺距补偿倍率为 1）(Magnification of PITCH for X)

N3624P#1R35；（X 轴螺距补偿点的间隔为 35）(Interval of PITCH for X axis)

N1851P#1R-1；（X 轴反向间隙补偿量为-1）(X axis backlash)

G11；（取消参数输入方式）

G10L50；（设定螺距输入方式）

N21R-6；（21 号螺距补偿量）(No. 21 data)

N22R-6；（22 号螺距补偿量）(No. 22 data)

N23R-6；（23 号螺距补偿量）(No. 23 data)

N24R-7；（24 号螺距补偿量）(No. 24 data)

N25R-7；（25 号螺距补偿量）(No. 25 data)

N26R-7；（26 号螺距补偿量）(No. 26 data)

N27R-7；（27 号螺距补偿量）(No. 27 data)

N28R-6；（28 号螺距补偿量）(No. 28 data)

N29R-7；（29 号螺距补偿量）(No. 29 data)

N30R-7；（30 号螺距补偿量）(No. 30 data)

G11；（取消螺距输入方式）

M30；

%

Y 轴补偿宏程序：

%

O8011；

G10L52；（设定参数输入方式）

#1=2（选择轴为 Y 轴）(Y axis)

N11502R00001100；（执行宏程序调用和可编程参数输入高速执行）
N3620P#1R100；（Y 轴参考点的螺距补偿点号为 100）(NO. of PITCH for Y)
N3621P#1R91；（Y 轴负方向最远端的螺距补偿点号为 91）(NO. of PITCH for -Y)
N3622P#1R100；（Y 轴正方向最远端的螺距补偿点号为 100）(NO. of PITCH for +Y)
N3623P#1R1；（Y 轴螺距补偿倍率为 1）(Magnification of PITCH for Y)
N3624P#1R35；（Y 轴螺距补偿点的间隔为 35）(Interval of PITCH for Y axis)
N1851P#1R6；（Y 轴反向间隙补偿量为 6）(Y axis backlash)
G11；（取消参数输入方式）
G10L50；（设定螺距输入方式）
N91R-5；（91 号螺距补偿量）(No. 91 data)
N92R2；（92 号螺距补偿量）(No. 92 data)
N93R0；（93 号螺距补偿量）(No. 93 data)
N94R7；（94 号螺距补偿量）(No. 94 data)
N95R3；（95 号螺距补偿量）(No. 95 data)
N96R7；（96 号螺距补偿量）(No. 96 data)
N97R-1；（97 号螺距补偿量）(No. 97 data)
N98R6；（98 号螺距补偿量）(No. 98 data)
N99R2；（99 号螺距补偿量）(No. 99 data)
N100R7；（100 号螺距补偿量）(No. 100 data)
G11；（取消螺距输入方式）
M30；
%

Z 轴补偿宏程序：
%
O8012；
G10L52；（设定参数输入方式）
#1=3（选择轴为 Z 轴）(Z axis)
N11502R00001100；（执行宏程序调用和可编程参数输入高速执行）
N3620P#1R80；（Z 轴参考点的螺距补偿点号为 80）(NO. of PITCH for Z)
N3621P#1R71；（Z 轴负方向最远端的螺距补偿点号为 71）(NO. of PITCH for -Z)
N3622P#1R80；（Z 轴正方向最远端的螺距补偿点号为 80）(NO. of PITCH for +Z)
N3623P#1R4；（Z 轴螺距补偿倍率为 4）(Magnification of PITCH for Z)
N3624P#1R27；（Z 轴螺距补偿点的间隔为 27）(Interval of PITCH for Z axis)
N1851P#1R28；（Z 轴反向间隙补偿量为 28）(Z axis backlash)

G11；（取消参数输入方式）
G10L50；（设定螺距输入方式）
N71R7；（71 号螺距补偿量）(No. 71 data)
N72R1；（72 号螺距补偿量）(No. 72 data)
N73R0；（73 号螺距补偿量）(No. 73 data)
N74R-2；（74 号螺距补偿量）(No. 74 data)
N75R3；（75 号螺距补偿量）(No. 75 data)
N76R0；（76 号螺距补偿量）(No. 76 data)
N77R-1；（77 号螺距补偿量）(No. 77 data)
N78R0；（78 号螺距补偿量）(No. 78 data)
N79R1；（79 号螺距补偿量）(No. 79 data)
N80R-2；（80 号螺距补偿量）(No. 80 data)
G11；（取消螺距输入方式）
M30；
%

附录三 PC 端软件自动生成的测量程序

X 轴测量程序：

```
%
O123
G01
G94
G90
F2000
G01 X+000.0000
M00
#1=0
#2=5
N0110
G01 X+005.0000
G04 X0.5
G01 X+000.0000
G04 X1.0
G01 X-035.0000
G04 X1.0
G01 X-070.0000
G04 X1.0
G01 X-105.0000
G04 X1.0
G01 X-140.0000
G04 X1.0
G01 X-175.0000
G04 X1.0
G01 X-210.0000
G04 X1.0
G01 X-245.0000
G04 X1.0
G01 X-280.0000
G04 X1.0
G01 X-315.0000
```

```
G04 X1.0
G01 X-350.0000
G04 X1.0
G01 X-355.0000
G04 X0.5
G01 X-350.0000
G04 X1.0
G01 X-315.0000
G04 X1.0
G01 X-280.0000
G04 X1.0
G01 X-245.0000
G04 X1.0
G01 X-210.0000
G04 X1.0
G01 X-175.0000
G04 X1.0
G01 X-140.0000
G04 X1.0
G01 X-105.0000
G04 X1.0
G01 X-070.0000
G04 X1.0
G01 X-035.0000
G04 X1.0
G01 X+000.0000
G04 X1.0
#1=#1+1
IF [#1 LT #2] GOTO 110
M30
%
```

Y 轴测量程序：

```
%
O123
```

```
G01
G94
G90
F2000
G01 Y+000.0000
M00
#1=0
#2=5
N0110
G01 Y+005.0000
G04 X0.5
G01 Y+000.0000
G04 X1.0
G01 Y-035.0000
G04 X1.0
G01 Y-070.0000
G04 X1.0
G01 Y-105.0000
G04 X1.0
G01 Y-140.0000
G04 X1.0
G01 Y-175.0000
G04 X1.0
G01 Y-210.0000
G04 X1.0
G01 Y-245.0000
G04 X1.0
G01 Y-280.0000
G04 X1.0
G01 Y-315.0000
G04 X1.0
G01 Y-350.0000
G04 X1.0
G01 Y-355.0000
G04 X0.5
```

```
G01 Y-350.0000
G04 X1.0
G01 Y-315.0000
G04 X1.0
G01 Y-280.0000
G04 X1.0
G01 Y-245.0000
G04 X1.0
G01 Y-210.0000
G04 X1.0
G01 Y-175.0000
G04 X1.0
G01 Y-140.0000
G04 X1.0
G01 Y-105.0000
G04 X1.0
G01 Y-070.0000
G04 X1.0
G01 Y-035.0000
G04 X1.0
G01 Y+000.0000
G04 X1.0
#1=#1+1
IF [#1 LT #2] GOTO 110
M30
%
```

Z 轴测量程序：

```
%
O123
G01
G94
G90
F2000
G01 Z+000.0000
```

```
M00
#1=0
#2=5
N0110
G01 Z+005.0000
G04 X0.5
G01 Z+000.0000
G04 X1.0
G01 Z-027.0000
G04 X1.0
G01 Z-054.0000
G04 X1.0
G01 Z-081.0000
G04 X1.0
G01 Z-108.0000
G04 X1.0
G01 Z-135.0000
G04 X1.0
G01 Z-162.0000
G04 X1.0
G01 Z-189.0000
G04 X1.0
G01 Z-216.0000
G04 X1.0
G01 Z-243.0000
G04 X1.0
G01 Z-270.0000
G04 X1.0
G01 Z-275.0000
G04 X0.5
G01 Z-270.0000
G04 X1.0
G01 Z-243.0000
G04 X1.0
G01 Z-216.0000
```

```
G04 X1.0
G01 Z-189.0000
G04 X1.0
G01 Z-162.0000
G04 X1.0
G01 Z-135.0000
G04 X1.0
G01 Z-108.0000
G04 X1.0
G01 Z-081.0000
G04 X1.0
G01 Z-054.0000
G04 X1.0
G01 Z-027.0000
G04 X1.0
G01 Z+000.0000
G04 X1.0
#1=#1+1
IF [#1 LT #2] GOTO 110
M30
%
```